Journal of Hydrology 604 (2022) 127272

Contents lists available at ScienceDirect

Journal of Hydrology

journal homepage: www.elsevier.com/locate/jhydrol

Research papers

Robust clustering for assessing the spatiotemporal variability of groundwater quantity and quality

Vahid Nourani [a,c,*], Parnian Ghaneei [a], Sameh A. Kantoush [b]

[a] Center of Excellence in Hydroinformatics and Faculty of Civil Engineering, University of Tabriz, 29 Bahman Ave., Tabriz, Iran
[b] Disaster Prevention Research Institute, Kyoto University, Goka-sho, Uji City, Kyoto 611-0011, Japan
[c] Near East University, Faculty of Civil and Environmental Engineering, Near East Boulevard, 99138, Nicosia, via Mersin 10, Turkey

ARTICLE INFO

This manuscript was handled by Gokmen Tayfur, Editor-in-Chief, with the assistance of Corrado Corradini, Associate Editor

Keywords:
Groundwater
Pollution Index of Groundwater (PIG)
Cluster ensemble
Ghorveh-Dehgolan Plain (GDP)

ABSTRACT

The long-term spatiotemporal assessment of groundwater resources through robust clustering techniques can be used to promote remediation measures for groundwater depletion and contamination. To fully understand the variability of groundwater quantity and quality due to anthropogenic activities and climate changes, a new ensemble clustering framework based on the Combining Multiple Clusters via Similarity Graph (COMUSA) method was developed. This new approach was applied and evaluated in the context of groundwater well systems on the Ghorveh-Dehgolan Plain (GDP), which is located in western Iran, for groundwater level (GWL) and 13 physicochemical parameters during four periods (the average of data from 1988–1990, 1997–1999, 2006–2008, and 2015–2017). The classification was confirmed by using the cluster validity index of the silhouette coefficient (SC), which indicated that the cluster ensemble method could improve the performance of individual clustering methods for groundwater quantity and quality by up to 12% and 20%, respectively. Piper plots, US Salinity Laboratory Staff (USSL) diagrams, and the pollution index of groundwater (PIG) were assessed for all clusters of physicochemical variables to analyse groundwater suitability for drinking and irrigation purposes. The results of the cluster ensemble showed that a critical pattern of groundwater depletion occurred in the western half of the GDP, while the eastern part was recognized as the most polluted zone on the plain. It could be concluded that the decline in GWL was not the only reason for the increase in groundwater quality variables, but other factors, such as noticeable cropland expansion and the overuse of chemical fertilizers and pesticides, were also influential factors related to these patterns. Taken together, the results of this study contribute to better recognizing the spatiotemporal changes in groundwater quantity and quality under the intense pressure of anthropogenic activities.

1. Introduction

Sustainable groundwater management is one of the significant issues in environmental engineering. While freshwater scarcity affects human life, there is also ample evidence suggesting that the quality of groundwater, the largest freshwater resource, is threatened due to the combination of industrial development, inadequate sanitation systems, chemical fertilizers and pesticides, and groundwater depletion. Groundwater depletion and contamination of aquifers affect human health, costs of water supplies, and future civilization; hence, recognizing changes in groundwater quantity and quality is an essential part of informed water resource protection.

Groundwater quality depends on changes in various variables, and spatiotemporal assessment of each variable is a complicated and time-consuming procedure. To simplify assessments of groundwater quality, decreasing the large dimension of water quality variables and representing data in a simpler way, various water quality indices have been proposed, which provide a simple value to identify the quality of water. For instance, the relative effect of each chemical variable on the general chemical quality of groundwater may be assessed using the pollution index of groundwater (PIG). This index quantifies the concentration status of water quality measures related to their standards for drinking water quality (e.g., see Subba Rao and Chaudhary, 2019; Egbueri, 2020).

Considering the importance of groundwater protection, finding efficient methods to recognize complex relationships between various

* Corresponding author at: University of Tabriz, 29 Bahman Ave., Tabriz 5166616421, Iran.
E-mail addresses: nourani@tabrizu.ac.ir (V. Nourani), kantoush.samehahmed.2n@kyoto-u.ac.jp (S.A. Kantoush).

https://doi.org/10.1016/j.jhydrol.2021.127272
Received 4 June 2021; Received in revised form 22 November 2021; Accepted 25 November 2021
Available online 4 December 2021

Table 1
Details of the reviewed papers, where the individual clustering methods were utilized.

Clustering method	Title	Findings	Author (year)
HCA	Groundwater quality assessment in a hyper-arid region of Rajasthan, India.	Cluster analysis by HCA proved to be an excellent tool to ascertain the spatial similarity between the contributing variables.	Bhakar and Singh, 2019
HCA	Groundwater quality assessment using pollution index of groundwater (PIG), ecological risk index (ERI) and hierarchical cluster analysis (HCA).	The efficiency and efficacy of PIG, ERI, and HCA in the drinking water quality assessments have been achieved.	Egburi, 2020
HCA	Hydrogeochemical processes regulating the spatial distribution of groundwater contamination, using pollution index of groundwater (PIG) and hierarchical cluster analysis (HCA).	The study suggests strategic management measures for sustainable development of groundwater resources.	Subba Rao and Chaudhary, 2019
K-Means	Cluster analysis for groundwater classification in multi-aquifer systems based on a novel correlation index.	Compared to the classical hydrogeological models and graphical approaches, the proposed methodology presents robust validation and results.	Fabbrocino et al., 2019
K-Means and SOM	Characterization of water quality conditions in the Klang River basin, Malaysia using self organizing map, and k-means algorithm.	The application of a combination of SOM and K-Means approaches extracted valuable information from the data for holistic river basin management.	Sharif et al., 2015
SOM	Hydrogeochemical characterization and quality assessment of groundwater using self-organizing maps in the Hangjinqi gasfield area, Ordos basin, NW China.	The results of the study can be used to investigate the seasonal variation of hydrogeochemical characteristics and assess water quality accurately.	Wu et al., 2021
SOM	Spatiotemporal variation of water pollution near landfill site: Application of clustering methods to assess the admissibility of LWPI.	The results showed that SOM could represent more precise results than principal component analysis (PCA) due to the ability to diagnose nonlinear patterns.	Baghanam et al., 2020
SOM	Self-organizing map clustering technique for ANN-based spatiotemporal modeling of groundwater quality parameters.	Spatial clustering via SOM was shown to be useful in improving FFNN-based modeling of groundwater quality parameters.	Nourani et al., 2016
GNG	Regional frequency analysis using growing neural gas network.	The results of the heterogeneity measure based on the L-moments approach reveal that only the GNG algorithm successfully yields homogeneous sub-regions in comparison to the K-Means, FCM, SOM, and WARD methods.	Abdi et al., 2017

variables is an essential step in extracting the most homogeneous patterns. Additionally, spatiotemporal assessments of these homogeneous patterns can effectively find and trace the time and place of changes in groundwater variables. In this regard, one of the robust multivariate analyses is clustering, which is widely used to classify multidimensional inputs into homogeneous groups. Clustering can extract features from an unlabelled input to form clusters having maximum within-group-object similarity and between-group-object dissimilarity (Nourani and Kalantari, 2010).

In general, all members of each cluster may be regarded to have almost the same pattern that can simplify evaluation and accelerate decision-making processes, for instance:

(i) A designed water resource management strategy for a member (e.g., watershed or piezometer) may also be applied to the other cluster members, which have similar conditions.
(ii) Variables of a hydrological model for a cluster member may further be verified for other members of that cluster.
(iii) The available data of a cluster may be used to fill in missing data of other members within the same cluster.

The powerful applications of clustering methods have encouraged researchers to take advantage of various clustering algorithms in groundwater assessment for specific purposes (Table 1). As a practical linear type of clustering, the K-Means algorithm has been applied to several hydrology fields due to the simple linear structure that can classify unlabelled inputs into separate K clusters (e.g., Fabbrocino et al., 2019; Sharif et al., 2015). Hierarchical cluster analysis (HCA) is another successful clustering approach developed as a powerful partitioning tool that seeks to build a hierarchy of clusters. Different HCA types (single linkage, complete linkage, average linkage, and WARD method) have yielded valuable results in groundwater assessment research (e.g., see Bhakar and Singh, 2019).

Some clustering algorithms utilize competitive learning concepts to classify data automatically, and one of the best-known examples is the self-organizing map (SOM). In the standard version of SOM, the number of neurons should be set based on the expected number of clusters. Previous studies have revealed that SOM is a powerful tool to visualize different groups of groundwater quality and quantity variables (see Wu et al., 2021; Baghanam et al., 2020; Nourani et al., 2016).

Although SOM has been widely applied for clustering purposes, the inefficiency in topology recognition is a major limiting factor of the SOM method. Another limitation of utilizing the SOM clustering method on large-scale structures of inputs is the time-consuming process of SOM. To diminish the impacts of these limiting factors, other alternative methods have been suggested on the basis of SOM. Growing neural gas (GNG) is an SOM-based algorithm that learns complex relationships without prior knowledge. GNG uses competitive Hebbian learning (CHL) to form topology without being restricted in k-dimensional structures. This method has gained considerable attention due to its flexibility in complex pattern recognition and has been successfully utilized as a multipurpose tool in various fields of engineering, such as robotics (Viejo et al., 2014), medicine (Aljobouri et al., 2018), the clothing industry (Jimeno-Morenila et al., 2016), hydrology (Abdi et al., 2017), and computer science (e.g., Shi et al., 2014; García-RodríGuez et al., 2012; Santos and Nascimento, 2016), but there is a gap in the use of GNG for the clustering and assessment of groundwater quality and quantity variables.

On the other hand, since every individual clustering method can extract particular features from a dataset and there is no agreement among researchers about the superiority of a specific method (Table1), finding an appropriate clustering method is a challenging task. Additionally, the homogeneous formation of clusters is a sensitive process in which the cluster ensemble can effectively perform and benefit from the advantages of different clustering methods simultaneously (e.g., see Mohammadi et al., 2008; Azimi et al., 2009; Mimaroglu and Erdil, 2011,

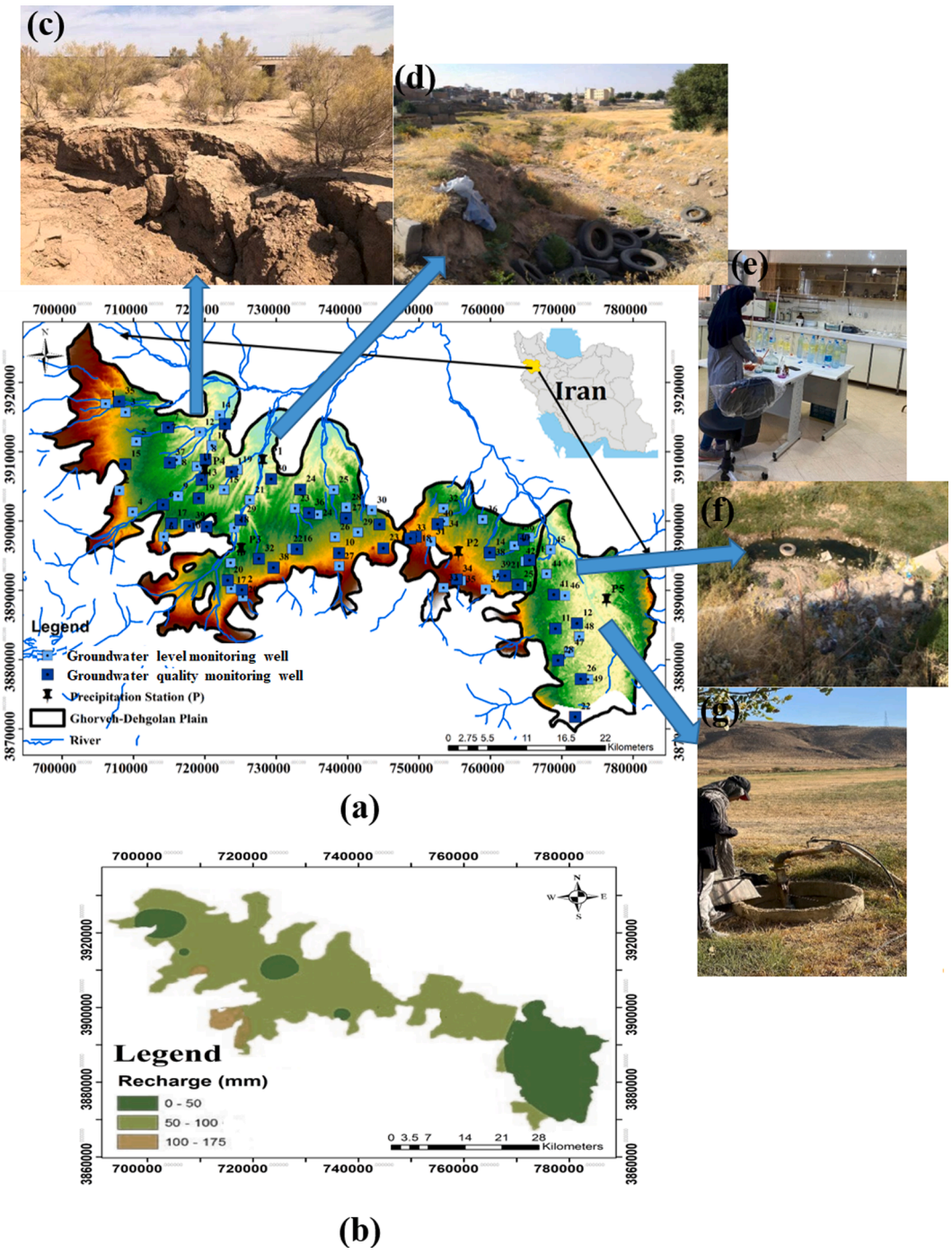

Fig. 1. Study area: Ghorveh Dehgolan Plain, Iran: (a) location map and positions of groundwater level monitoring wells and groundwater quality monitoring wells, (b) distribution of aquifer recharge, (c) subsidence in the northwestern part of GDP, (d) Dehgolan's dried up river, (e) water quality assessment laboratory, (f) leachate footprint in the eastern part of GDP, (g) quality monitoring well 12 in GDP.

Mimaroglu and Erdil, 2013). Combining multiple clustering via similarity graph (COMUSA) is a flexible cluster ensemble method that creates a similarity graph by utilizing the evidence accumulated from the different clustering methods. COMUSA can find arbitrarily shaped clusters and is not affected by cluster size, noise, or outliers, leading to more homogeneous clusters (Mimaroglu and Erdil, 2011). There are still no studies that have applied the COMUSA algorithm in the general fields of hydrology and water resources.

The present study attempted to identify spatiotemporal groundwater quantity and quality changes using ensemble clustering based on the similarity graph method for the Ghorveh-Dehgolan Plain (GDP), located in western Iran, where overpumping and overuse of fertilizers and pesticides for irrigational purposes have placed significant pressures on groundwater resources of the GDP. This method was applied to combine the results of three practical clustering algorithms (commonly used K-Means method, agglomerative hierarchical method of Ward, and GNG as an unsupervised ANN-based method) to extract the most homogeneous structures of clusters from groundwater variables of the GDP. After recognizing existing groundwater quality and quantity patterns, the Piper plot, US Salinity Laboratory Staff (USSL) diagrams, and PIG evaluated the quality of patterns to investigate groundwater suitability for drinking and irrigation purposes.

Table 2
Statistics of GWL and physicochemical variables data for the GDP.

Time step	Variable	GWL	K^+	Na^+	Mg^{2+}	Ca^{2+}	Cl^-	HCO_3^-	CO_3^{2-}	NO_3^-	SO_4^{2-}	TH	EC	pH	TDS
1 (1988–1990)	Unit	m	mEq/L	mEq/L	mEq/L	mEq/L	mEq/L	mEq/L	mEq/L	mEq/L	mEq/L	mg/L	μZ/cm	–	mg/L
	Max	1958	0.21	2.22	2.09	4.4	0.64	6.26	0.11	1.24	1.36	244	685	8.28	444
	Min	1769	0.01	0.25	0.76	2.15	0.16	2.65	0	0.12	0.21	122	312	7.9	200
	Average	1844	0.03	0.66	1.05	3.02	0.32	3.8	0.05	0.34	0.59	172	465	8.13	298
	SD	41.30	0.04	0.49	0.28	0.54	0.11	0.74	0.03	0.21	0.30	36.59	90.5	0.09	58.65
2 (1997–1999)	Max	1959	0.36	2.92	3.09	7.66	0.81	10.08	0.1	1.24	2.49	537.3	1046.3	8.26	680.25
	Min	1770	0.01	0.22	0.63	1.89	0.15	2.45	0	0.12	0.01	133	311.3	7.45	199.3
	Average	1845	0.03	0.76	1.24	3.40	0.34	4.31	0.01	0.35	0.42	232.4	484.7	8.05	313.2
	SD	41.28	0.06	0.59	0.47	0.93	0.18	1.24	0.02	0.19	0.59	67.32	138.3	0.16	90.18
3 (2006–2008)	Max	1959	0.17	3.26	3.91	5.99	0.87	7.83	0.73	1.292	2.87	451.2	981.7	8.24	643.67
	Min	1762	0.01	0.23	0.66	2.04	0.13	2.14	0	0.12	0.18	142.7	306	6.78	194.6
	Average	1833.5	0.03	0.86	1.19	3.20	0.29	3.83	0.08	0.35	0.73	219.9	481.4	7.95	308.18
	SD	43.88	0.03	0.73	0.64	0.98	0.18	1.38	0.12	0.19	0.72	77.4	157.3	0.30	102.38
4 (2015–2017)	Max	1957	0.57	6.78	8.39	15.39	3.25	23.38	0.22	1.37	4.4	1189	2475.2	8.26	1658.2
	Min	1736	0.01	0.27	0.44	1.74	0.08	2.59	0	0.1	0.09	109	296.6	6.23	188.8
	Average	1820	0.04	1.17	1.33	3.58	0.36	4.84	0.02	0.37	0.57	246	556.3	7.82	359.80
	SD	48.92	0.09	1.18	1.44	2.55	0.51	3.92	0.04	0.22	0.77	196	388	0.44	261.33
Whole period (1988–2017)	Max	1961	0.343	3.431	3.963	9.314	1.514	13.58	0.563	8.053	4.752	666	1312	8.52	863
	Min	1740	0.007	0.244	0.625	1.955	0.106	0	0	0.119	0.113	138	306.2	6.685	195
	Average	1839	0.029	0.853	1.219	3.289	0.349	4.115	0.042	0.412	0.621	225	499.2	7.99	321
	SD	48.98	0.101	0.262	0.256	0.382	0.193	0.368	0.128	0.115	0.309	24.903	65.117	0.110	67.47

2. In situ experimental investigation on the study area and data analysis

The GDP is located in western Iran within the longitude from 47° 38′ 52″ to 48° 06′ 03″ east and latitude from 35° 02′ 22″ to 35° 30′ 54″ north. The climate of the examined area is semiarid, while during winter, the average minimum temperature is 5.5 °C, and the region experiences a daily maximum temperature of 36 °C in the summer. Moreover, the average annual precipitation in this area is 345 mm. This paper used data of 49 groundwater level monitoring wells in the plain for monitoring monthly GWL and 41 groundwater quality monitoring wells, measured twice a year, for monitoring geochemical variables provided by the Kurdestan Regional Water Authority (KRWA, 2017). The location map and positions of wells of the GDP are shown in Fig. 1a. The main recharge sources of groundwater of GDP are precipitation and subsurface flow from surrounding highlands and rivers (Fig. 1b), while the semiarid climate with low precipitation and surface water potential limit the recharge process of the aquifer. In addition, irrigation water infiltrates back to the groundwater system. The northwestern parts of the plain have experienced extreme subsidence due to the high amounts of groundwater depletion (Fig. 1c). Besides, anthropogenic activities have impacted the plain, which drained a large part of surface water resources such as the Dehgolan river (Fig. 1d). Groundwater samples of the GDP were tested in a laboratory to examine the physicochemical variables to study the water quality (Fig. 1e). The plain also has hygienic problems because there is no sanitary landfill in the region (Fig. 1f), resulting in leachate penetration into groundwater. There are several observation wells in the plain to explore and collect water samples for studying the groundwater quantity and quality (Fig. 1g).

In this study, four time steps with ten-year intervals were selected to investigate long-term trends of data sets. Due to the possibility of extreme values in a 1-year dataset, the average of three-year datasets for each time step was selected to avoid possible bias and anomalies. A statistical summary of the groundwater parameters is presented in Table 2.

The unconfined alluvial aquifer of GDP covers an area of approximately 1270 km^2 in Kurdistan Province. Based on pumping tests carried out in the plain, the transmissivity of the GDP aquifer varies between 50 and 1492 m^2/d. The range of hydraulic conductivity of the aquifer is from 34 to 90 m/day. The average value of the GDP aquifer storage coefficient is about 1.7%. GWLs vary from 1740 m to 1961 m above the mean sea level. The GDP is located in the Sanandaj-Sirjan structural zone of Iran. The Sanandaj-Sirjan is identified as a region of polyphase deformation, the latest reflecting the collision of Arabia and Eurasia and the subsequent southward propagation of the fold-thrust belt. Therefore, the geology of the study area is characterized by geologic structures and fracture systems. Geological examinations have shown that this area primarily contains limestone-dolomite rocks and Quaternary units, the most common of which include alluvial-plain deposits, alluvial terraces, alluvial-fan deposits, calcareous sandstone, and travertine. Notably, small areas with dolomite and limestone were discovered in the central and western parts of the plain, which are susceptible to pollution caused by transportation on land surfaces, which flow into the aquifer (karst system) to a large extent (Rahmati et al., 2015). Fig. 2 also contains geological cross-sections indicating possible structures in the GDP. Fine-grained and coarse-grained units are repeated alternately over the plain and do not follow a specific order regarding the condition of borehole logs of exploratory wells in GDP. Fig. 3 shows some samples of borehole logs in the western part (L1, L2, and L3), central part (L4, L5, and L6), and eastern part (L7, L8, and L9) of the GDP, illustrating the direct relationship between the increase in depth and the coarse-grained units. Hydrogeological properties of the aquifer layers and their thickness were estimated through 340 geoelectrical soundings and 15 geo-electrical profiles provided by KRWA (KRWA, 2017); see Fig. 4, representing three of them.

Fig. 4a illustrates the western section (i-i′), including four layers. The first layer shows the surface layer with a thickness of 15–40 m containing alluvial deposits consisting of silt, clay, sand, and gravel. The samples of boreholes show the soil textures of the first layers of the i-i′ section (Fig. 3b). The second layer thickness varies from 25 to 50 m, forming from the alternation of medium-grained alluvial at the top and coarse-grained alluvial deposits at the deeper depth. The main texture of the third layer is fine-grained alluvial deposits with an average depth of 50 m. The third layer with a lower potential of discharge contains groundwater. The fourth layer is the bedrock of this profile, referring to the Terissic-Jurassic period, and contains dark grey crystalline limestone with interbedded metavolcanic rocks, slate, phyllite, conglomerate, and crystalline limestone. Geophysical investigations divided the central profile (ii-ii′) into three layers (Fig. 4b). The first layer with a thickness range of 5–30 m is an alternation of surface alluvial deposits with high percents of gravel. The second layer thickness reaches 200 m, in which the alluvial deposits with high percents of gravel were recognized. The last layer as bedrock contains granite, amphibole granite, diorite, marble, and crystalline dolomite. In some areas of the ii-ii′ cross-section,

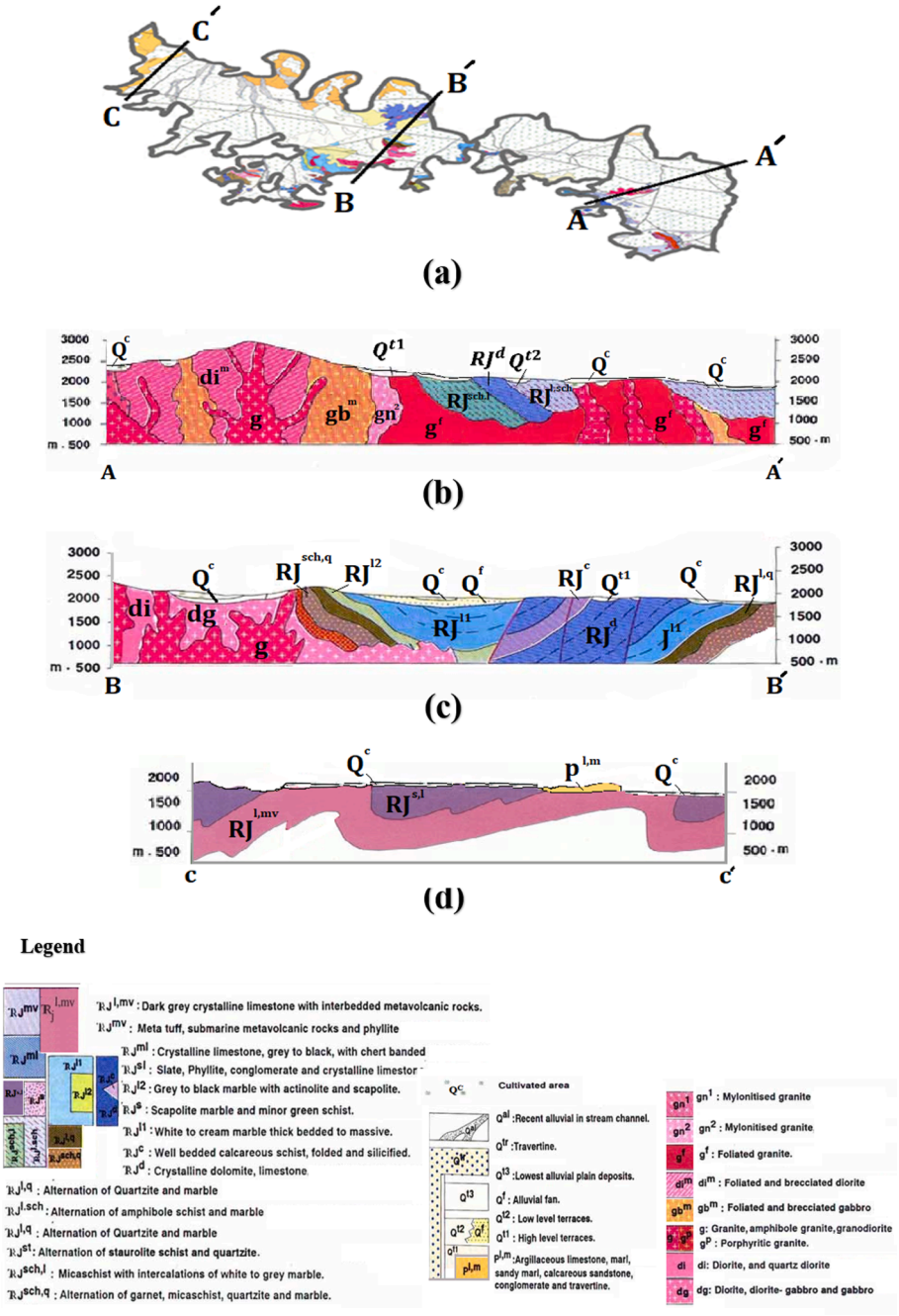

Fig. 2. Geological map of the GDP: (a) plan, (b) cross-section in the A-A′ direction, (c) cross-section in the B-B′ direction, and (d) cross-section in the C-C′ direction.

the bedrock is not detected due to the existence of a fault creating a significant disturbance in the lower alluvium of the aquifer. The first layers of the eastern cross-section (iii-iii′, Fig. 4c) consist of alternations of fine-grained alluvial deposits with high percents of silt, clay, and gravel (see borehole logs of Fig. 3d). The bedrock of the eastern part of the GDP's aquifer has low resistivity representing layers such as argillaceous, marl, and sandy marl. It is worth mentioning that the low groundwater quality of the eastern part of GDP could affect and disturb the results of geophysical investigations.

In order to define groundwater flow directions and rates through the aquifer, the interpolation map of GWL was created regarding the permeability of the aquifer materials. The Kriging algorithm was utilized to create an interpolation map and generate contour maps (Fig. 5). Each contour, or equipotential, represents a line of equal hydraulic head. It is clear from Fig. 5 that the general groundwater flow direction is from the west and southwestern regions of the plain to the east and southeastern regions. Also, the southern parts of the aquifer have greater hydraulic gradients and the location of equipotential lines represent a lower groundwater hydraulic gradient in the eastern part of GDP.

3. Methodology

Utilizing the proposed methodology of this study (see Fig. 6), groundwater quantity and quality variables of the GDP were first patterned using three individual clustering methods: K-Means, Ward, and GNG; then, the cluster ensemble technique was used as a post-processing method to form the most homogeneous clusters. Additionally, before assessing the conditions of clusters, cropland expansion was visualized by using the normalized difference vegetation index (NDVI) data of all time steps to show its impacts on groundwater on the GDP.

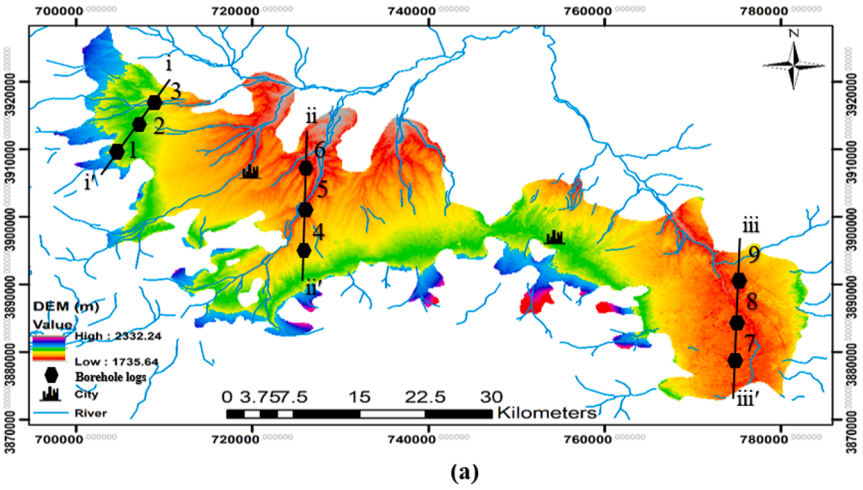

(a)

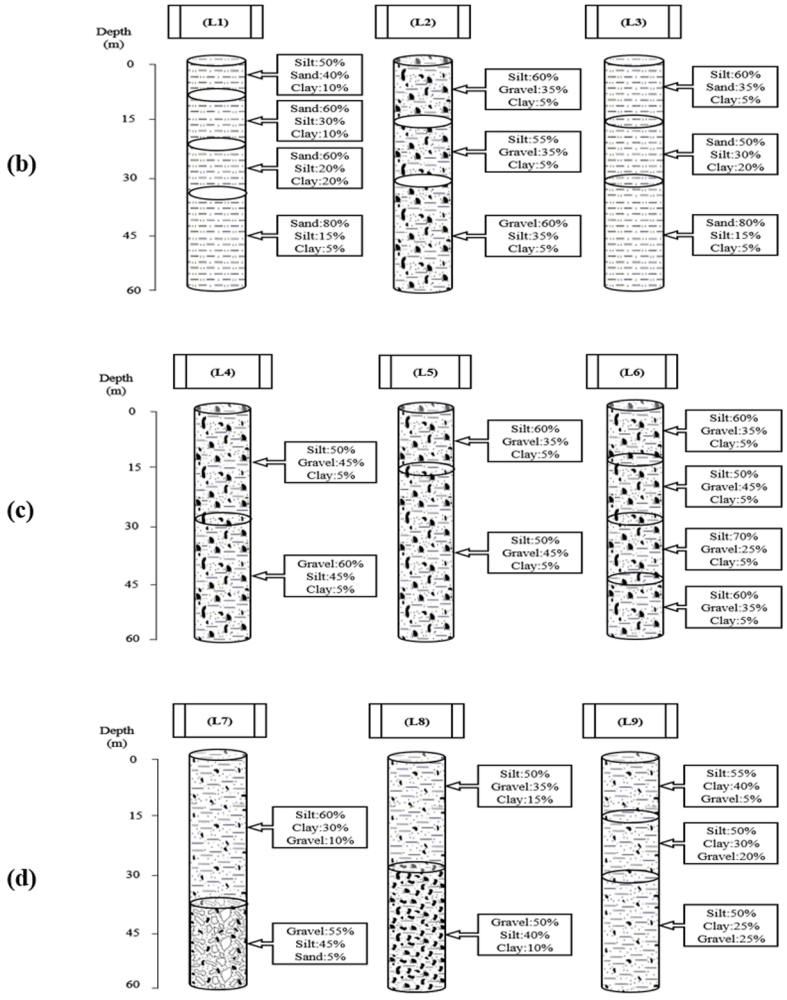

Fig. 3. Borehole logs: (a) logs positions and digital elevation model, (b) logs of the western part (L1, L2, and L3), (c) logs of the central part (L4, L5, and L6) and (d) logs of eastern part (L7, L8, and L9) of GDP.

Finally, spatiotemporal analyses of the patterns obtained were conducted by comparing groundwater level (GWL), PIG, Piper, and USSL diagrams.

3.1. K-Means clustering method

K-Means is one of the clustering methods that has shown decent performance in hydrological research. K-Means classifies inputs into clusters in which the distance between the members and the centroid of clusters is at a minimum degree (MacQueen, 1967). Finally, this algorithm aims at minimizing an objective function given by:

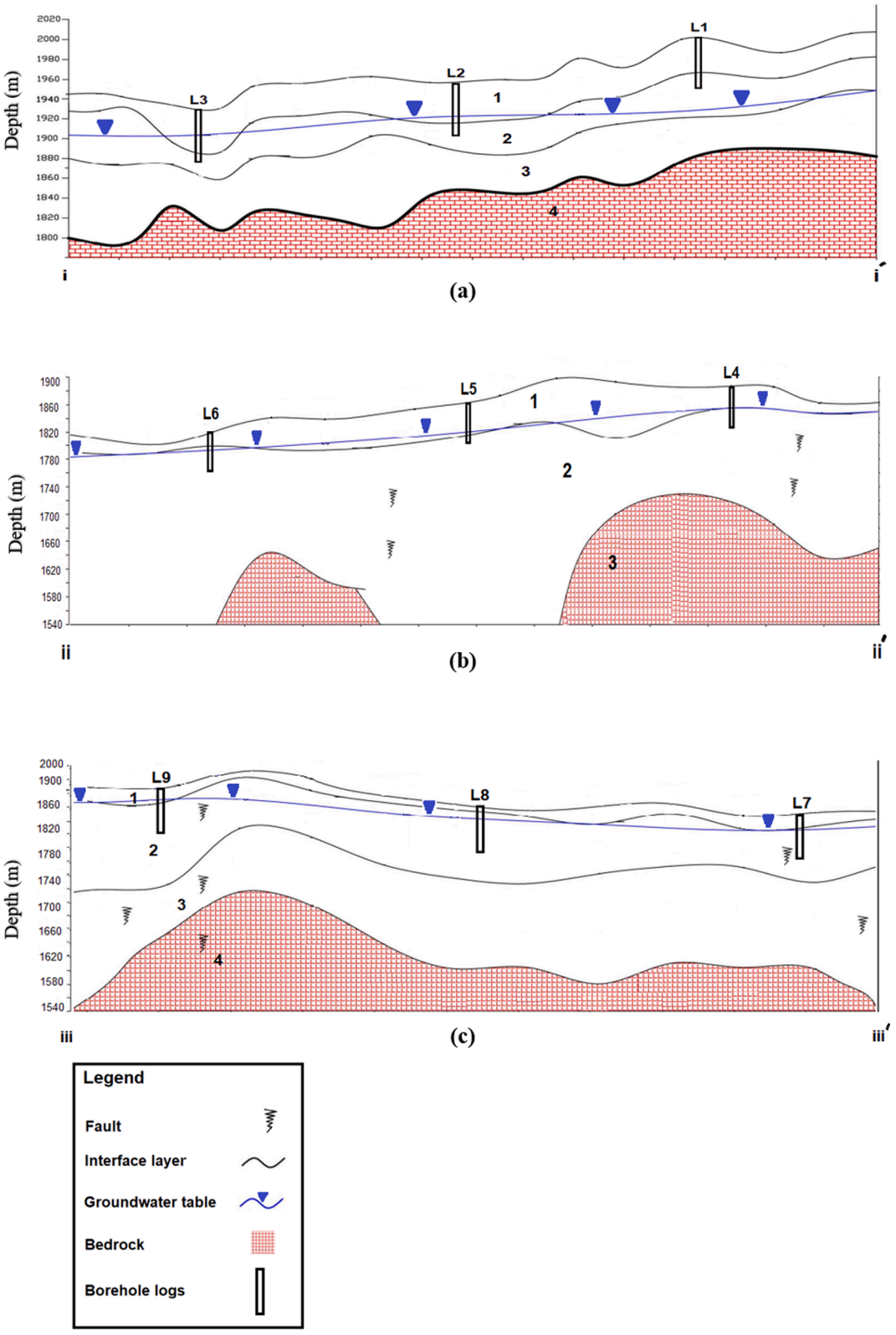

Fig. 4. Hydrogeological cross-sections: (a) western, (b) central, and (c) eastern hydrogeological cross-sections of GDP.

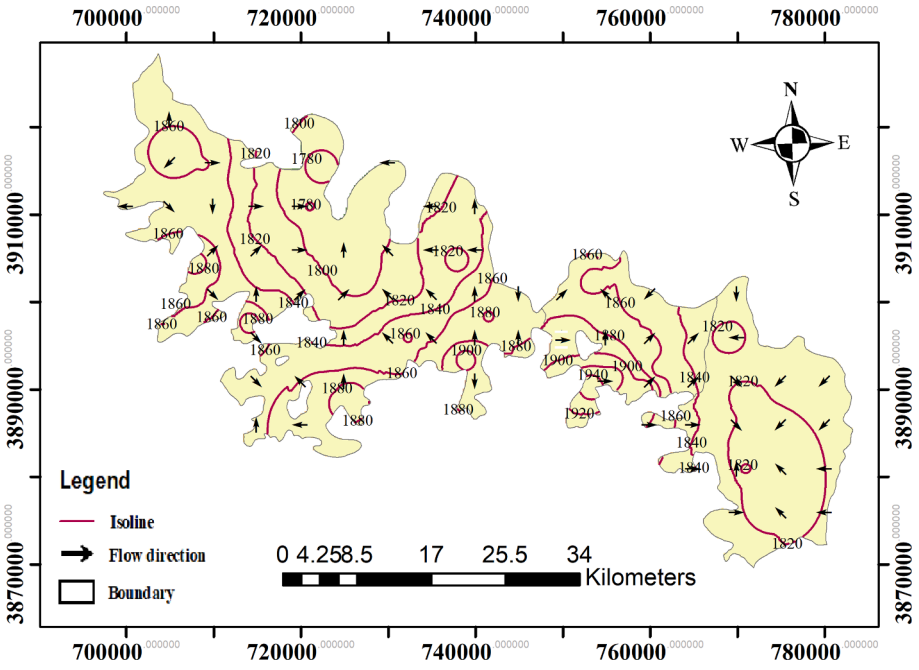

Fig. 5. Groundwater flow system of the GDP.

$$J = \sum_{i=1}^{N}\sum_{j=1}^{K} r_{nk}(\|x_i - v_j\|)^2 \quad (1)$$

where N is the number of data points, K is the number of clusters, $\|x_i - v_j\|$ is the Euclidean distance between x_i and v_j, $r_{nk} \in \{0,1\}$ is indicator variable where k describing the data point x_i is assigned to which of the K clusters, x is the set of data points, and v is the set of centres.

3.2. Ward's hierarchical clustering method

Hierarchical cluster analysis has been developed as a flexible data-grouping application in scientific fields. This method first forms clusters with a single member, then these clusters are merged to create clusters containing two members, and this process continues until it forms a final cluster consisting of all members. New clusters are created based on the minimum variance of each step (for more details about the hierarchical clustering method, see Subba Rao and Chaudhary, 2019; Egbueri, 2020).

3.3. Growing neural gas (GNG) network

GNG is one of the SOM-based algorithms that, as an unsupervised learning method, further utilizes a growing mechanism for gradual adaptation. To create a network topology without being restricted in a k-dimensional structure, GNG utilizes the CHL growth approach (Fritzke, 1995). Linking neurons form the neighbourhood network, which structures in each iteration by first- and second-winner neurons at random positions and associated reference vectors. Then, GNG generates a random input related to a density function, and finding the nearest neurons (winner neurons), continues to increase the age of all edges. The insertion of connections between the two closest neurons to the randomly generated input patterns establishes an induced Delaunay triangulation in the input space. The elimination of connections diminishes the edges that no longer comprise the triangulation. This is performed by eliminating the connections between neurons that are no longer close or that have nearer neurons. Finally, the accumulated error allows the identification of those zones in the input space where it is necessary to increase the number of neurons to improve the mapping (Jimeno-Morenilla et al., 2013).

The GNG-learning algorithm steps are as follows (Fig. 7):

i. Start with neuron a and neuron b at random positions in which w_a and w_b are their associated reference vectors.
ii. Generate a random input time series related to a density function $P(\xi)$.
iii. Find the nearest neuron s_1 (winner neuron) and the second nearest neuron s_2.
iv. Increase the age of all edges emanating from s_1 to its neighbours.
v. Increase the local error of s_1 by using the Euclidean distance between two vectors as $\Delta error(s_1) = \|W_{(s_1)} - \xi\|^2$ (2)
vi. Relocate s_1 and its topological neighbours towards ξ by ε_w and ε_n (learning rates), respectively, of the total distance (n shows all direct neighbours of s_1):

$$\Delta W_{s_1} = \varepsilon_w(\xi - W_{s_1}) \quad (3)$$

$$\Delta W_{s_n} = \varepsilon_n(\xi - W_{s_n}) \quad (4)$$

vii. If there exists an edge between s_1 and s_2, then set zero as their age.
viii. Remove the edges larger than a_{max}. If this results in isolated neurons (without emanating edges), remove them as well.
ix. For every certain number of inputs generated, insert a new neuron.
x. Decrease all error variables by multiplying them with a constant β.
xi. Delete outliers based on the network edge length average.
xii. If the stopping criterion is not yet achieved, proceed to step 2.
xiii. Reorder network neurons using neighbourhood structure.

Unlike classical clustering algorithms, GNG has a flexible and adaptable algorithm that makes it practical for learning the topology of high-dimensional datasets. The GNG algorithm was written and implemented in MATLAB R2018b.

3.4. Combining multiple clusterings via similarity graph (COMUSA)

Cluster ensemble methods aim to combine multiple clustering algorithm results to produce a better clustering outcome than those from

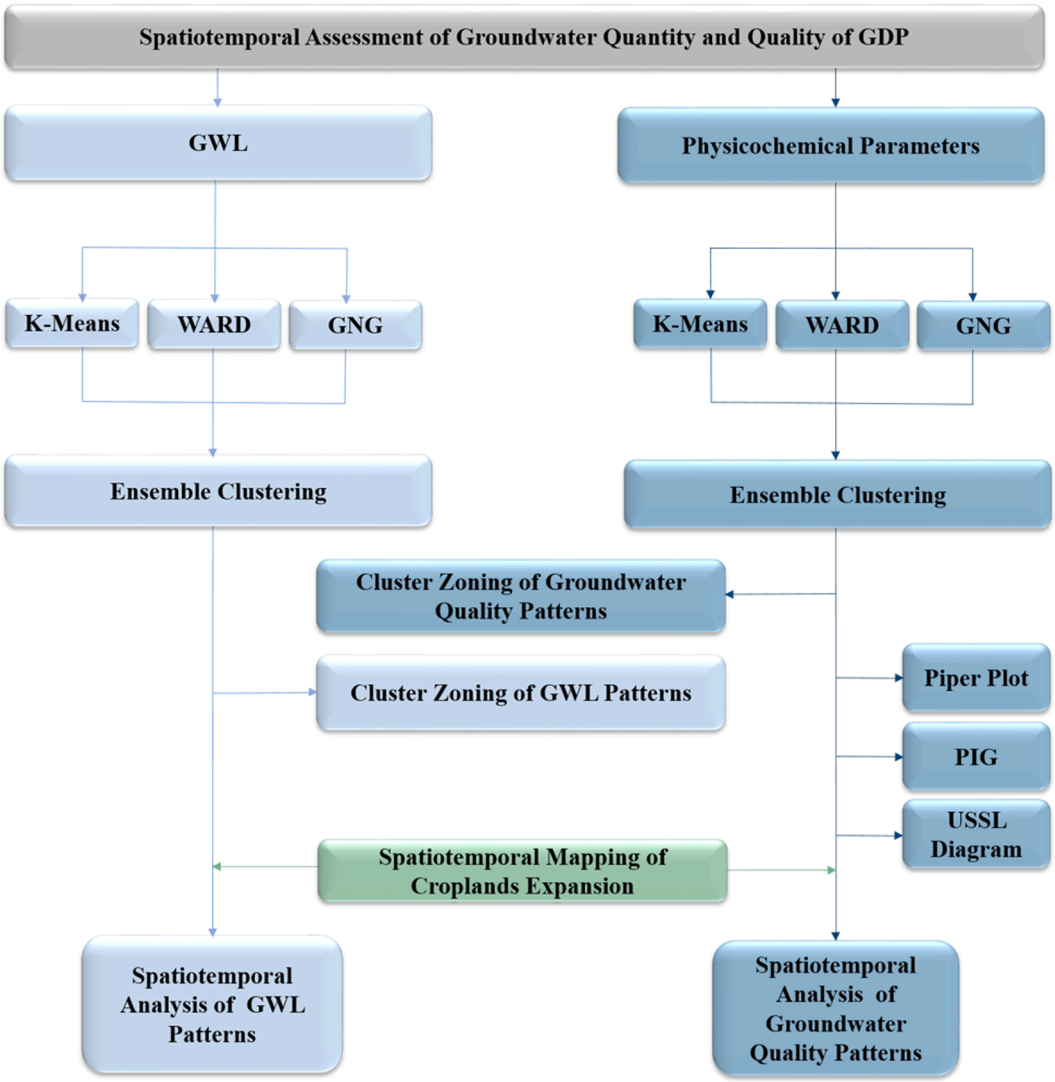

Fig. 6. Schematic diagram of the proposed methodology for groundwater quantity and quality assessment in four time steps.

individual clustering methods in terms of consistency and quality. Combining multiple clustering methods requires reusing pre-existing knowledge, employing distributed data-mining methods, and producing a final clustering with better overall quality. Various solutions for combining multiple clustering methods have been presented, such as genetic, hybrid bipartite graph formulation, hypergraph partitioning, and *meta*-clustering algorithms (Alqurashi and Wang, 2019). There is no single algorithm that is universally used, and there are no generally agreed upon criteria for selecting the most suitable ones. In this case, it is better to apply the one with the most simplicity and efficiency.

With this aim, the present study attempted to combine the three clustering methods in groundwater assessment using the similarity graph method via the following steps (Mimaroglu and Erdil, 2011):

where D is a dataset:

$\pi(D) = \{C_1.C_2.\bullet\bullet\bullet.C_{\pi(D)}\}$ is an individual clustering of D; C_i is a cluster of $\pi(D)$; $\pi(D)=\{\pi_1(D), \pi_2(D), \ldots,\pi_m(D)\}$ is a set of the best results of different clustering methods.

The following function forms a co-association (similarity) matrix (SM):

$$coassoc(i.j) = votes_{i.j} \tag{5}$$

where $votes_{i.j}$ is the number of times that members i and j were in the same clusters. This information of members produces the SM. The similarity graph is an undirected and weighted graph that displays the SM. In a similarity graph, SG=(D,E), and each edge $(d_i.d_j)$ has a mark associated with the SM_{ij} in the co-association matrix. df (d_i) is the degrees of freedom, and sw(d_i) is the sum of weights of edges incident to d_i. The attachment index (Eq. (6)) is for initiating new clusters. A member with the highest attachment index is selected as an initial member (pivot).

$$attachment(d_i) = \frac{\mathrm{sw}(d_i)}{\mathrm{df}(d_i)} \tag{6}$$

Initially, each cluster is a singleton, and the pivot object expands the cluster by considering all immediate neighbours. A neighbour is included in a pivot's cluster if it is most similar to the pivot. Once a neighbour is included, it is marked and then acts like a pivot by considering its immediate neighbours for further expansion. Each cluster is expanded by its neighbours as explained previously. Extension of a cluster comes to an end if pivots of a cluster cannot add any other objects into the cluster. COMUSA starts a new cluster by choosing a new pivot if there are unmarked objects in a dataset. COMUSA halts when all objects are marked (for more details, see Mimaroglu and Erdil, 2011). Note that the COMUSA algorithm was written and implemented in MATLAB R2018b.

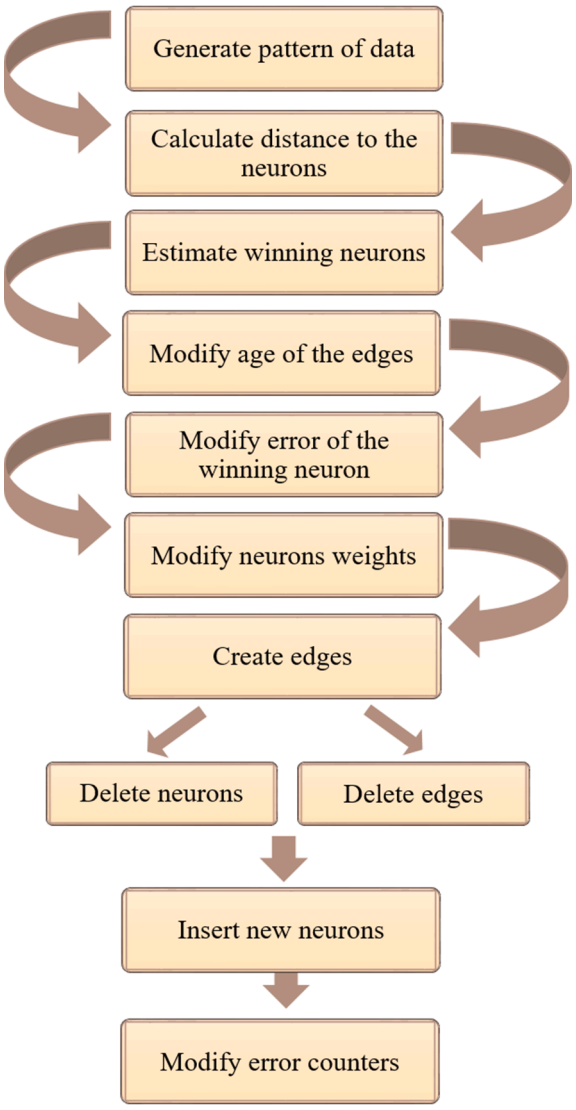

Fig. 7. Flow chart of GNG-learning algorithm.

3.5. Cluster validity index

The silhouette coefficient (SC) is measured to assess and compare the performance of clustering methods. To calculate the SC for clustering structures, first, the S_i for all members is calculated as a silhouette index (Rousseeuw, 1987):

$$S_i = \frac{b(i) - a(i)}{max\{a(i).b(i)\}} \tag{7}$$

$a(i)$ is the average Euclidean distance between member i and all members of cluster A, and $b(i)$ is the least average dissimilarity of member i to the members within a cluster distinct from cluster A. Based on this formula, it infers that $-1 \leq S_i \leq 1$. Therefore, if S_i is adjacent to 1, it may be concluded that the S_ith feature vector has been allocated to a proper cluster. Conversely, when S_i is adjacent to -1, it may be inferred that the S_i th feature vector has been classified incorrectly. When S_i is almost zero, it indicates that the S_i th feature vector is located similarly far away from two clusters.

While n is the number of members, and k is the number of clusters, the overall quality of a clustering method and the optimal number of clusters can be validated using the average silhouette width of the entire dataset for each number of clusters as:

Table 3
Relative weight, weight variable, and drinking water quality standard limits (Subba Rao and Chaudhary, 2019).

Variable	Units	R_W	Wp	Ds
pH		5	0.128	7.5
TDS	mg/L	5	0.128	500
TH	mg/L	3	0.077	300
Ca^{2+}	mg/L	2	0.051	75
Mg^{2+}	mg/L	2	0.051	30
Na^{+}	mg/L	4	0.103	200
K^{+}	mg/L	1	0.026	12
HCO_3^-	mg/L	3	0.077	300
Cl^-	mg/L	4	0.103	250
SO_4^{2-}	mg/L	5	0.128	200
NO_3^-	mg/L	5	0.128	45
$\sum$ sum		39	1	–

$$SC = \max_k \left(\frac{1}{n} \sum_1^n S_i \right) \tag{8}$$

When average silhouette values were calculated for desired numbers of clusters ($k \in \{2, 3, \cdots, n\}$) the maximum average silhouette is SC representing the optimal number of clusters. A higher SC illustrates better discrimination among the clusters.

3.6. Pollution index of groundwater (PIG)

Subba Rao (2012) proposed the PIG to quantify pollution activity originating from anthropogenic and geogenic sources in which the relative effect of single chemical variables on the general chemical quality of groundwater can be identified by using only a simple value (Subba Rao, 2012).

Suitability assessment of drinking water quality by using the PIG is taken in five steps:

i. Estimation of the relative weight (R_w) (on a scale of 1–5) of the analyzed variables based on their significance in the water quality assessment and relative impact on human health (Table 3).
ii. Calculation of the weight parameter (Wp) to assess its relative association with the groundwater quality (Table 3) is as follows:

$$W_P = \frac{R_W}{\sum R_W} \tag{9}$$

iii. The status of concentration (Sc) is measured by dividing each of the water quality variable contents (C) by its respective drinking water quality standard limits (Ds) as:

$$Sc = \frac{C}{D_s} \tag{10}$$

Table 3 presents the status of the relative influence of individual physicochemical variables on overall groundwater quality by using Rw, Wp, and Ds.

iv. The overall groundwater quality (Ow) is calculated by multiplying the Wp by the Sc.

$$OW = W_p \times Sc \tag{11}$$

v. The summation of all Ow values per sample gives the PIG as:

$$PIG = \sum OW \tag{12}$$

The PIG values reveal the contributions of all analyzed hydrochemical variables of each groundwater sample. It is noteworthy that in

Table 4
Results of individual clustering methods based on the SC in all time steps.

	Clustering Method	Time Step							
		1		2		3		4	
		NC	SC	NC	SC	NC	SC	NC	SC
Groundwater Level	**WARD**	2	0.57276	2	0.60073	4	0.65679	8	0.61331
	K-Means	2	0.60028	3	0.65046	4	0.65018	7	0.62075
	GNG	3	0.61366	3	0.65996	5	0.65936	7	0.62161
Quality Variables	**WARD**	3	0.47934	3	0.47385	2	0.71476	3	0.64390
	K-Means	3	0.49934	2	0.47459	2	0.71597	3	0.68439
	GNG	3	0.50835	3	0.50444	2	0.72203	3	0.71832

this study, in addition to the variables in Table 3, the sodium absorption ratio (SAR) and electrical conductivity (EC) parameters also contributed to the evaluation of groundwater suitability for irrigational purposes.

4. Results and discussion

Assessment of hydrological phenomena has complicated procedures where analysis requires powerful applications of enhanced methods and to that end, in this study, first, to explore and assess the spatiotemporal changes of groundwater quantity and quality on the GDP, the study was conducted over four time steps. The first, second, third, and fourth-time steps are the averages of the datasets for the 1988 to 1990, 1997 to 1999, 2006 to 2008, and 2015 to 2017 limits, respectively. The averages of three years as representative of the time steps were selected to avoid possible bias and anomalies that may occur in a one-year dataset. The groundwater quantity and quality datasets of these four time steps were first clustered separately by individual clustering methods, and the optimal results were selected based on the SC. With the aim of enhancing the structure of clusters, the results of individual clustering methods were then combined through a cluster ensemble algorithm as a post-processing step. Finally, the spatiotemporal changes of clusters were evaluated via the assessment of the SC, GWL, PIG, and groundwater quality diagrams.

4.1. Results of individual clustering methods

Individual clustering algorithms, including linear (K-Means), hierarchical (WARD), and self-organizing neural network (GNG) clustering methods, were applied to the four time step datasets, and the optimal number of clusters (NC) was chosen by comparing the SC from 2 to 10 clusters after the training process. The results of individual clustering methods are shown in Table 4 for GWL and physicochemical variables (using normalized data).

As shown in Table 4, in all time steps, the SC indicates better performance for the GNG clustering method compared with the other individual clustering methods. The main reason for the superiority of GNG against WARD and K-Means is the way that this flexible method can drive its nodes through the topology of inputs. In contrast, the rigid structure of the other methods (K-Means and WARD) limits their applicability in dealing with complex datasets. Additionally, the adaptation ability and optimized growth of GNG lead to a desired resolution of the clustered networks.

Based on the SC, results higher than 0.5 show well-structured clusters, and those lower than 0.5 show that samples are structured poorly. A comparison of SC values in Table 4 indicates the satisfactory performance of all clustering methods in GWL clustering. In contrast, the SC values of qualitative clustering via K-Means and WARD methods illustrate inadequate structures in some time steps. These differences between the SC of quantitative and qualitative clustering might be related to the number of input variables. For GWL clustering, only spatial parameters (UTM) and groundwater level were imposed on clustering algorithms, while in qualitative clustering in addition to GWL variables, 13 physicochemical variables of groundwater samples were utilized.

Table 5
Results of the cluster ensemble of all time steps for GWL.

Time Step	SC	Members of cluster
1	0.64049	W1, W2, W3, W4, W5, W6, W10, W16, W17, W20, W22, W26, W28, W29, **W30**, W31, W32, W34, W36, W38, W39, W40, W41, W42 W7, W8, W9, W11, W12, W13, W14, W15, **W18**, W19, W21, W23, W24, W25, W43, W44, W45, W46, W47, W48, W49 W27, **W33**, W35, W37
2	0.67771	W1, W2, W3, W4, W5, W6, W10, W17, W22, W26, W28, W29, **W30**, W31, W32, W34, W36, W38, W39 W7, W8, W9, W11, W12, W13, W14, W15, W16, **W18**, W19, W20, W21, W23, W24, W25, W27, W40, W41, W42, W43, W44, W45, W46, W47, W48, W49 **W33**, W35, W37
3	0.67104	W1, W2, W6, W17, W20, **W27**, W31 W3, W4, W5, W7, W10, W16, W22, W26, W28, W29, **W30**, W32, W34, W36, W38 W8, W9, W11, W12, W13, W14, W15, **W18**, W19, W21, W23, W25 W39, W40, W41, W42, W43, W44, W45, W46, W47, **W48**, W49 **W33**, W35, W37
4	0.65860	W1, W3, **W10** W2, W6, W17, W20, **W27** W4, W5, W7, W11, W16, W22, W24, **W28** W8, W9, W12, W13, W14, W15, **W18**, W19, W21, W23, W25 W29, **W30**, W32, W34, W36, W38 **W33**, W35, W37 W39, W40, W41, W42, W43, W44, W45, W46, W47, **W48**, W49

*The underlined letters represent the centroid well of each cluster.

The high-dimensional dataset of qualitative variables and the existence of nonlinear and complex relationships among variables caused unsatisfactory results in the K-Means and WARD methods. Under the same conditions, the GNG method obtained acceptable results in all time steps because of its ability to recognize complex relationships.

After applying individual clustering techniques, a cluster ensemble method was applied to improve the clustering performance as a post-processing step.

4.2. Results of the cluster ensemble

Regarding the fact that there is no agreement regarding the superiority of specific clustering methods and the optimal number of clusters, in this study, the best results of individual clustering methods were combined via the similarity graph (COMUSA) method, which can efficiently find the natural number of clusters (Mimaroglu and Erdil, 2011). With the similarity matrix formation for all time steps, the attachment index for all members was calculated. The highest amount was randomly selected based on the preliminary nodes of the clustering operation. Then, the correlation coefficient of other members related to the preliminary nodes was measured to form new clusters. This practice was continued until all members were settled in their clusters. COMUSA can

Table 6
Results of the cluster ensemble of all time steps for physicochemical variables.

Time Step	SC	Members of cluster
1	0.55604	W1, W2, W5, W6, W7, W8, W9, W10, W13, W14, W15, W16, W17, W18, W19, W20, W21, W22, W23, W25, W27, **W28**, W31, W32, W34, W35, W36, W37, W38, W39, W40 W3, W11, **W12**, W26, W29, W33 W4, **W24**, W30, W41
2	0.56881	W1, W2, W4, W5, W6, W7, W8, W9, W10, W11, W13, W14, W15, W16, W17, W18, W19, W20, W21, W22, W23, W25, W26, **W28**, W29, W30, W31, W32, W34, W35, W36, W37, W38, W39, W40 W3, **W12**, W24, W27, W33, W41
3	0.76809	W1, W2, W4, W6, W7, W8, W9, W10, W13, W14, W15, W16, W17, W18, W19, W20, W21, W22, W23, **W24**, W25, W27, W29, W30, W31, W32, W33, W34, W35, W36, W37, W38, W39, W40 W3, W11, **W12**, W26, W28, W41
4	0.73977	W1, W2, W3, W4, W6, W7, W8, W9, W10, W13, W14, W15, W16, W17, W18, W19, W20, W21, W22, W23, **W24**, W25, W27, W29, W30, W31, W32, W33, W34, W35, W36, W37, W38, W39, W40, W41 W11, W26, **W28** **W12**

*The underlined letters represent the centroid well of each cluster.

find shapes of clusters and can assign members to a cluster if they are most similar to a pivot (high attachment values) in that cluster. The growth of clusters is based on immediate neighbours of pivots. If a member enters a cluster, it receives a label as a new pivot to continue the expansion process of the cluster until all members are labelled, then COMUSA halts. Information on the quantitative and qualitative patterns of the cluster ensemble is presented in Tables 5 and 6. Additionally, as an example of generating a cluster ensemble using COMUSA, the final GWL clusters of the fourth-time step are shown in Fig. 8.

The red dotes in Fig. 8 highlight the preliminary pivot objects of all clusters, which indicate high attachment values, high sum of weights, and low degrees of freedom that indicate they are strongly connected somewhere. After estimating the pivot object, the expansion of each cluster is continued by considering all their immediate neighbours, shown with black circles (Fig. 8).

Furthermore, the Euclidean distance criterion was then calculated to determine the prominent (centroid) well of each cluster as the best representation of the groundwater quantity and quality clusters. The determined central wells of clusters are highlighted in the third column in Tables 5 and 6.

After recognizing the new patterns of GWL and physicochemical variables, the SC was computed for all time steps. A comparison of results in Table 4 with results in Tables 5 and 6 indicates that the application of the cluster ensemble could successfully enhance the performance of individual clustering methods for groundwater quality and quantity up to 12% and 20%, respectively. It is worth mentioning that an increase in the SC, even in small amounts, can be very effective in evaluating groundwater conditions. In areas where the number of observation wells is low, belonging to an appropriate cluster is crucial in making the decision about a member.

According to Tables 5 and 6, the centroid wells were almost the same until the number of clusters changed. It is noteworthy that the centres of the preliminary clusters have continued to maintain their position in later time steps, which indicates the suitability of the centroid wells to consider their quantitative and qualitative conditions as the best representative of clusters.

To provide a broader perspective on the impacts of anthropogenic activities on groundwater patterns, the areas of cropland expansion were assessed for all time steps. Additionally, the NDVI dataset of each time step was sketched to see the spatiotemporal changes in cropland and their impacts on the groundwater conditions on the GDP.

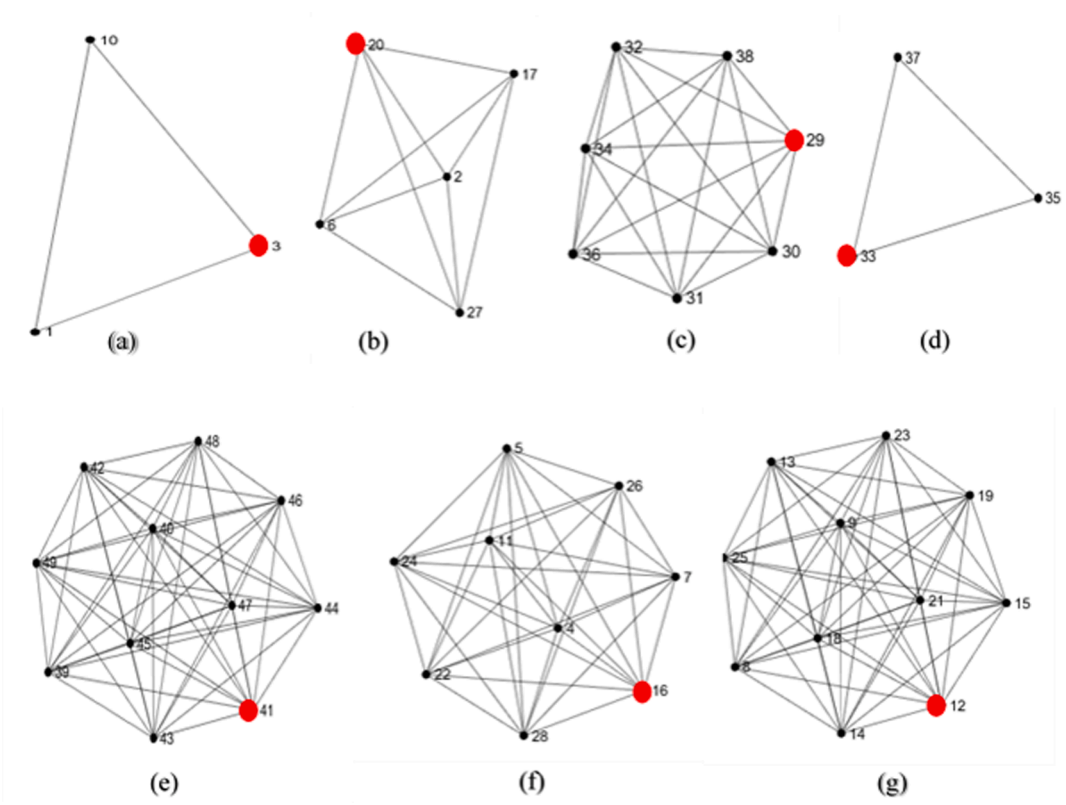

Fig. 8. Similarity graphs using the cluster ensemble method for GWL using COMUSA for the last-time step: (a) cluster 1, (b) cluster 2,…, and (g) cluster 7 (preliminary pivot objects).

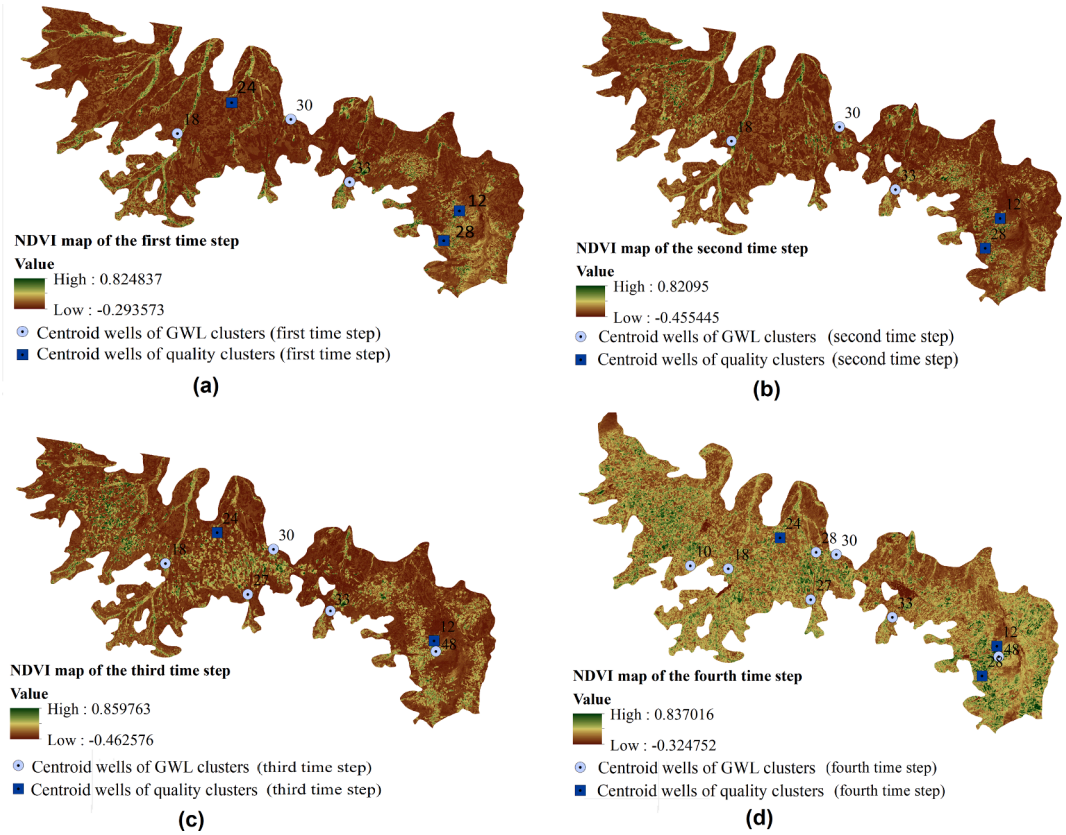

Fig. 9. NDVI maps of the (a) first, (b) second, (c) third and (d) fourth-time steps.

Table 7
Rainfed and irrigated cropland areas of all time steps on the GDP.

Time Step	Rainfed cropland area (ha)	Irrigated cropland area (ha)
1	103,016	17,655
2	151,834	28,501
3	140,876	39,695
4	160,399	42,330

4.3. Assessment of cropland areas

It is noteworthy that people living on the GDP depend on commodities produced by irrigated agriculture, and the GDP is one of Iran's potato production bases where farmers apply large amounts of water, fertilizers, and pesticides to agricultural soil to achieve a high production. Therefore, before assessing the quantitative and qualitative conditions of groundwater, having a broader perspective on cropland areas on the GDP is a valuable step in understanding the relationship between groundwater problems and cropland expansion on the GDP. Considering that the primary groundwater consumption on the GDP is for irrigational purposes, there can be a significant relationship between cropland expansion and groundwater problems which also has been reported for other regions in previous studies (e.g., Foroumandi et al., 2022). To this end, remote sensing (RS) can help visualize cropland area changes. Ground covers have a defined spectral signature (spectral reflectance patterns) compressed into spectral vegetation indices because of their ability to distinguish different vegetated surfaces. The NDVI is one of the most well-known vegetation indices and involves the ratio of the difference and the sum between near-infrared and red bands. This index can distinguish vegetation from other soil coverings (Nourani et al., 2021; Foroumandi et al., 2021).

To take into account the contribution of agricultural prosperity and its impacts on the quantitative and qualitative conditions of groundwater, the Landsat-derived NDVI maps related to July 1989, 1998, 2007, and 2016 (the spatial resolution size of 30 m for each pixel of Landsat-5 and Landsat-8 images) were sketched on the Google Earth Engine (GEE) cloud computing platform. The NDVI maps for all four time steps in which the darker green colours in pixels express the higher values of the NDVI, and the centroid wells of GWL and groundwater quality clusters are shown in Fig. 9.

According to reports from the agricultural organization of Kurdistan Province (Table 7), an incremental increase in irrigated cropland areas has occurred over time, which has almost more than doubled in the last-time step. Additionally, in the western half of the GDP, the irrigated cropland area increased over 90 percent between the second and third-time steps. These changes are clearly discernible among the maps in Fig. 9.

The difference in the area of irrigated cropland from 1988 to 2017 was 24,675 ha (Table 7). The most significant increase in irrigated cropland area occurred between the second and third-time steps (approximately 11194 ha). In comparison, the rainfed cropland area decreased by 10,958 ha during this time, which shows an increasing tendency among local farmers to cultivate irrigated crops. This crop pattern has shifted to cultivating water-intensive crops such as potato and forage crops, which is another influential factor affecting groundwater conditions on the GDP. The comprehensive assessment of cropland area changes and their impacts on groundwater status is performed simultaneously with trend analysis of clusters in the following subsections.

4.4. Trend analysis of GWL

The cluster ensemble of the GWL could recognize three patterns for both the first and second-time steps and could extract five and seven patterns for the third and fourth-time steps, respectively. The increase in the number of clusters indicates that, over time, initial strong

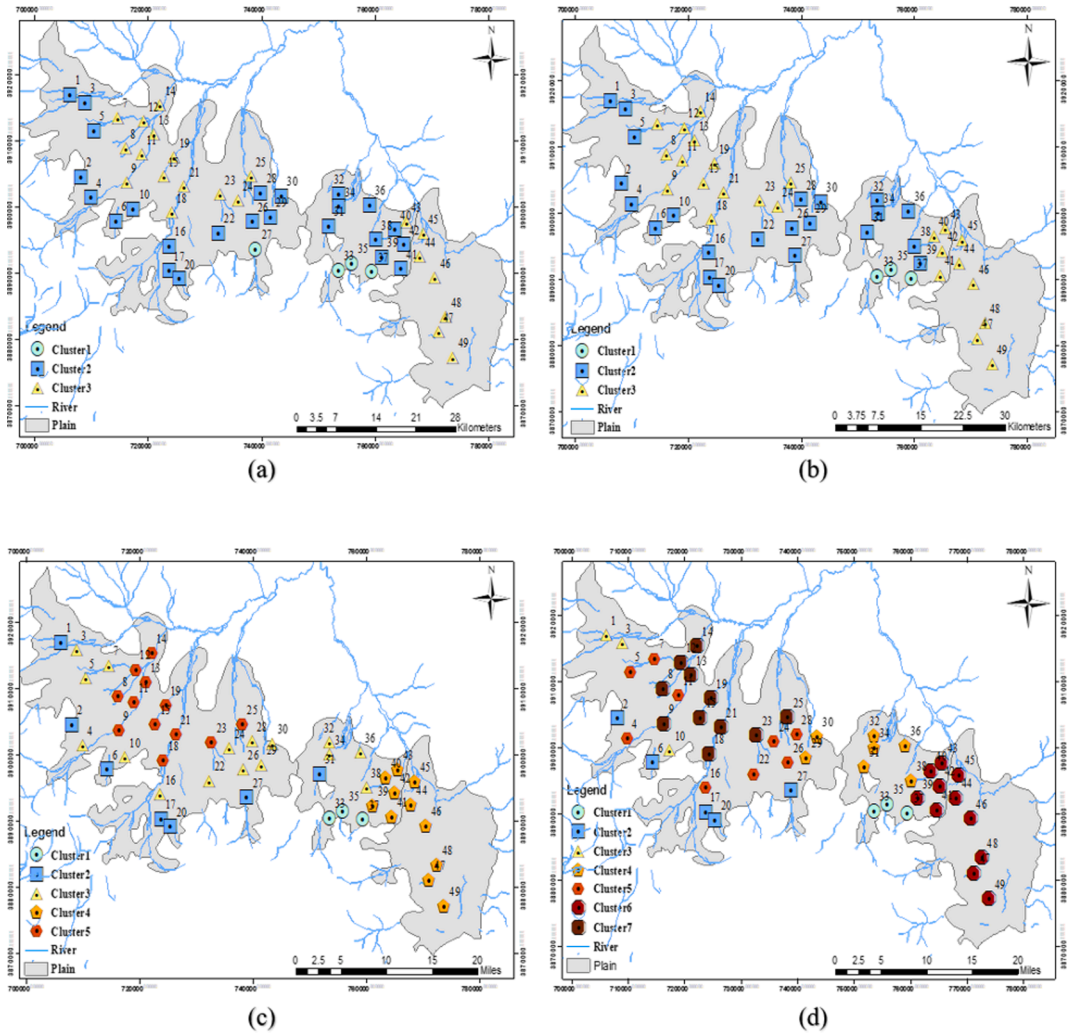

Fig. 10. Spatial distribution of GWL clusters in the (a) first, (b) second, (c) third and (d) fourth-time steps.

relationships among members have diminished and has resulted in splitting large clusters into smaller clusters to maintain the quality of the clusters. Fig. 10 shows the spatial distributions of the GWL clusters in the first and last-time steps.

As shown in Fig. 10a, GWL shows three patterns on the GDP in the first-time step, among which cluster 3, with the lowest GWL average (1805 m), was located in the eastern and northwestern parts of the plain. In the second-time step, the total GWL average of the plain increased by approximately 1 m, which could have been a consequence of the longest wet period on the GDP, which occurred from March 1994 to April 1996, and could have compensated groundwater overextraction. Comparison of the first two time steps indicates that clusters of GWL did not experience a significant change in the structure of clusters during this period (Fig. 10a and 10b). In the third-time step (Fig. 10c), the highest amounts of groundwater depletion (approximately 24 m) occurred in the western part of the GDP, where cluster 3 was split into two clusters. Between the second and third-time steps, the area of cropland increased significantly (Fig. 9), which could have changed the groundwater consumption pattern (the number of clusters rose to five during this time) in combination with climate change and population growth. Recognizing and forming new patterns from a cluster in the following years could have resulted from heterogeneous changes between members. Understanding these changes among the cluster members is one of the valuable outcomes of spatiotemporal cluster analysis. This application makes the time and place of uncommon events approximately recognizable.

In the last-time step, the number of recognized patterns was increased to seven, and the total distribution of members among clusters was changed, as shown in Fig. 10d. This relocation of members between clusters indicates the existence of inconsistent changes in the zones of these clusters, and one of the main factors was extensive groundwater withdrawal. On the other hand, crop patterns changed in which more water-intensive crops were cultivated, which could have significantly increased groundwater withdrawals. The most noticeable groundwater depletion (almost 24 m) during this time step is in cluster 7, located in the western part of the GDP. It is worth mentioning that from 1988 to 2017, the centroid well of cluster 7 (W18) experienced an almost 33 m decline on average. Eventually, the spatiotemporal comparison of GWL reveals that the zone of clusters with high amounts of groundwater depletion has expanded from the west and east to the centre of the GDP.

Since the wells that lie in the same cluster may have a similar pattern, the behaviour of wells in a cluster may be determined from an assessment of the central well utilized as the representative for groundwater conditions in the cluster (Nourani et al., 2016).

To visualize the trend of cluster changes over time and to investigate the relationship between the SC and the quantitative status of GWL clusters, the temporal changes of these factors are plotted for centroid wells selected as the best representatives in their respective clusters using the Euclidean distance criterion. Thus, wells 18, 30, 33, and 48 were chosen to have prominent representations of groundwater in the entire GDP. Fig. 11 shows the temporal changes in the GWL and SC of the centroid wells to show the impacts of agricultural prosperity on GWL in each pattern. The values of the variables were normalized before

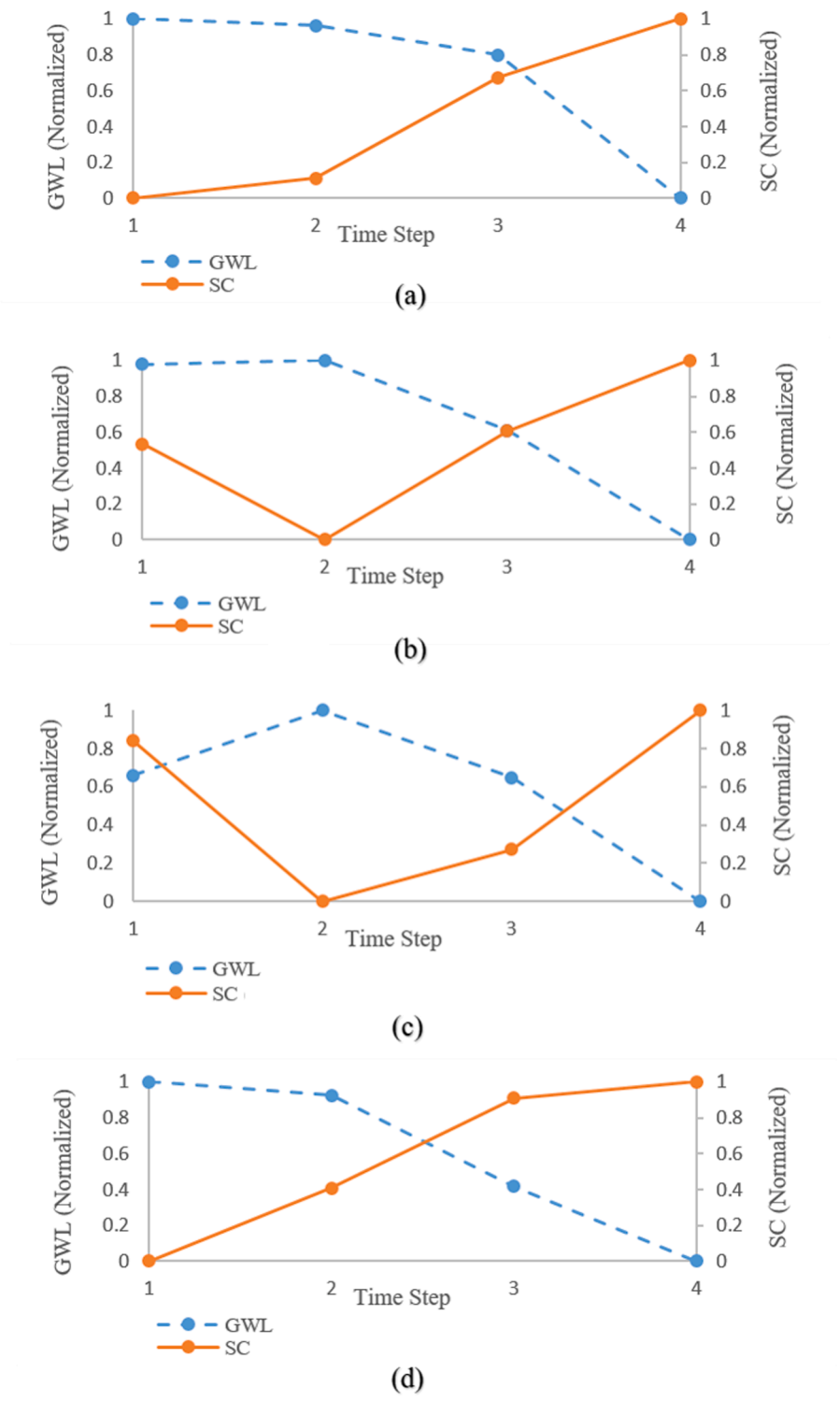

Fig. 11. The temporal changes of GWL and SC of centroid wells for clusters (a) W18, (b) W30, (c) W33, and (d) W48.

plotting.

It can be seen from all plots in Fig. 11 that the inverse relationship between the SC and GWL was maintained during the study period, which indicates that GWL depletion trends led to improved structures in these clusters (increase in the SC). These improvements resulted from the formation of clusters with higher within-group-object similarity and between-group-object dissimilarity. Based on the sharp decrease in GWL in most members, their similarities increased and consequently led to an increase in the SC. It could be concluded that with the increase in anthropogenic activities (e.g., excessive withdrawal of groundwater for irrigation purposes, which is a major consumer on the GDP), the natural diversity of GWL distribution on the GDP has been gradually decreasing, which can cause irreversible consequences, such as permanent subsidence and related ground failures, if the decline continues for a long period of time.

Well 18 was selected as a cluster representative for the western part of the GDP. As shown in Fig. 11a, the highest decrease in GWL (19 m) occurred between the third and fourth time steps. Over the period

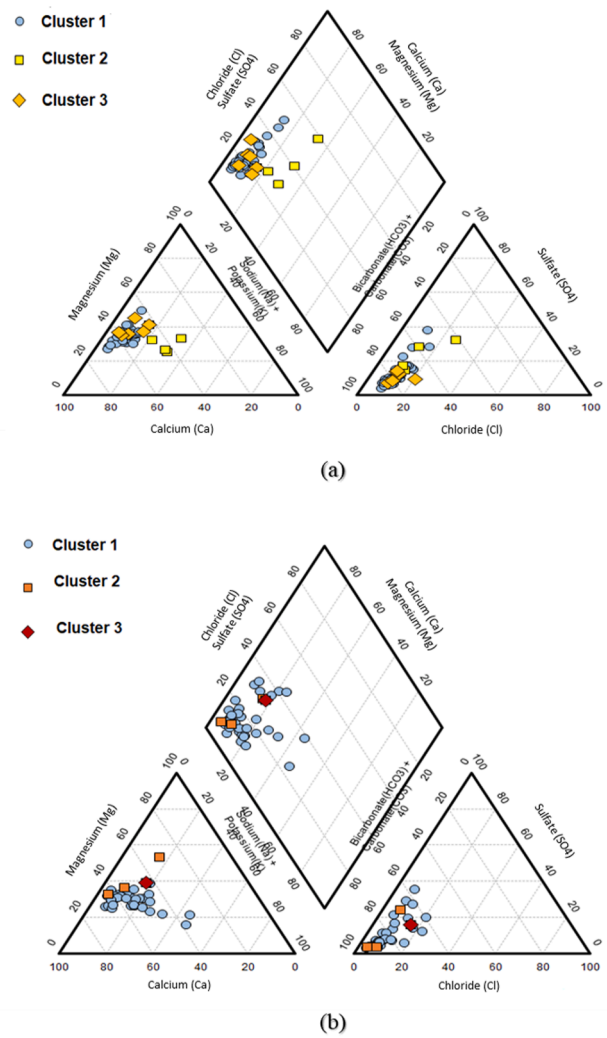

Fig. 12. The Piper diagrams of the (a) first and (b) fourth-time steps.

between the second and third time steps, despite the high increase in cropland areas, there was no large water-level drop because, during this period, the longest wet period of the region occurred and partially offset groundwater overpumping for agricultural activities. In contrast, after the second time step, this region underwent the most critical cluster with a decreasing trend in GWL.

Well 30 represents the cluster that was first located in the southwestern and centre parts of the GDP. Fig. 11b shows that the GWL of well 30 slightly increased between the first and second-time steps. The occurrence of the longest wet period (from March 1994 to April 1996) could have been a reason for the GWL increase during this time period. Increasing the GWL reduced the SC values, which indicates that the natural diversity of the GWL distribution has increased across the plain. The comparison of the first and last-time steps shows that the GWL of well 30 has decreased by approximately 33 m.

Well 33, with a 1.8 m depletion in GWL between the first and last-time steps, is the representative member of a small cluster located in the southern part of the GDP. In terms of GWL, this member had the smallest fluctuations compared with other centroid wells. Fig. 11c clearly shows that the inverse relationship between the GWL and SC remained even during small fluctuations in GWL.

Well 48 is the centroid member of the first eastern cluster with a 26-m depletion in which the GWL had a decreasing trend during all time steps, as shown in Fig. 11d. It is clear from Fig. 9 that the eastern part of the GDP between the first and last-time steps underwent a noticeable increase in cropland area that caused further intensification in the competition for groundwater resources.

Overall, the plots in Fig. 11 indicate that some factors, such as significant irrigated cropland expansion, lack of surface water resources, and GWL decline, might lead to a loss of natural diversity of GWL distribution on the GDP after the second-time step (1999).

4.5. Trend analysis of groundwater quality

Piper diagrams have been widely utilized to recognize the dominant hydrochemical facies by plotting major cation and anion concentrations (Piper, 1994). In the Piper diagram, major ions are plotted in two base triangles as major cations (Ca^{2+}, Mg^{2+} and$Na^{+}+K^{+}$) and major anions (Cl^{-}, SO_4^{2-}, and$CO_3{}^{2-}+HCO_3^{-}$) in milliequivalent percentages, and the diamond part shows the dominant water chemistry type. Based on the statistics of physicochemical variables in this study (Table 2), the order of dominant cations and anions are ranked as $Ca^{2+} > Mg^{2+} > Na^{+} > K^{+}$ and $HCO_3{}^{-} > SO_4{}^{2-} > NO_3{}^{-} > Cl^{-}$, respectively. Fig. 12 shows Piper diagrams plotted for all cluster members in the first and last-time steps in which the dominant facies of clusters are Ca–Mg-HCO3 and the dominance of weak acidic anions over strong acidic anions and alkaline earths over alkali anions are shown. The members that belong to the mixed-type zone can be recognized as neither cation nor anion dominant. Comparing the Piper plots related to the first and last-time steps (Fig. 12) shows the increase in $HCO_3{}^{-}$ in some clusters that could have been a consequence of soil CO_2 leakage to the groundwater. Organic matter decay and root respiration increase the soil CO_2 leakage rate, and the combination of CO_2 with groundwater recharge forms $HCO_3{}^{-}$, leading to mineral dissolution. Additionally, it is clear from Fig. 12 that the Na^{+} of some members increased over time steps, which could represent anthropogenic pollution footprints, such as a consequence of cropland expansion on the GDP.

Cluster ensemble of physicochemical variables could recognize three patterns for both the first and fourth-time steps and could extract two patterns for the second and third-time steps. To evaluate the water quality of clusters used specifically for drinking purposes, the PIG was calculated for each cluster by calculating the average PIG for the centroid wells in the clusters (see Table 8). The ranges of drinking water pollution have been categorized into five groups: PIG values below 1.0 indicate insignificant pollution (IP), 1.0–1.5 indicate low pollution (LP), 1.5–2.0 indicate moderate pollution (MP), 2.0–2.5 indicate high pollution (HP) and PIG > 2.5 indicate very high pollution (VHP) (Subba Rao, 2012).

The results show that until 2008 (third-time step), all clusters had an insignificant pollution level; hence, their qualities were suitable for drinking consumption despite increasing PIG values (Table 8). In the last-time step, the PIG values significantly increased in wells 12 and 28 (eastern part of the plain, Fig. 13), and their categories changed to low and high pollution. The assessment of the PIG for the last-time step indicates that the proposed method in this study could find exclusively

Table 8
Results of groundwater quality classification based on the PIG.

Time Step	1			2		3		4		
Centroid Well	W28	W24	W12	W28	W12	W24	W12	W24	W28	W12
PIG	0.5745	0.5328	0.8213	0.4888	0.8841	0.5500	0.8109	0.4626	1.375	2.02
Category	IP	IP	IP	IP	IP	IP	IP	IP	LP	HP

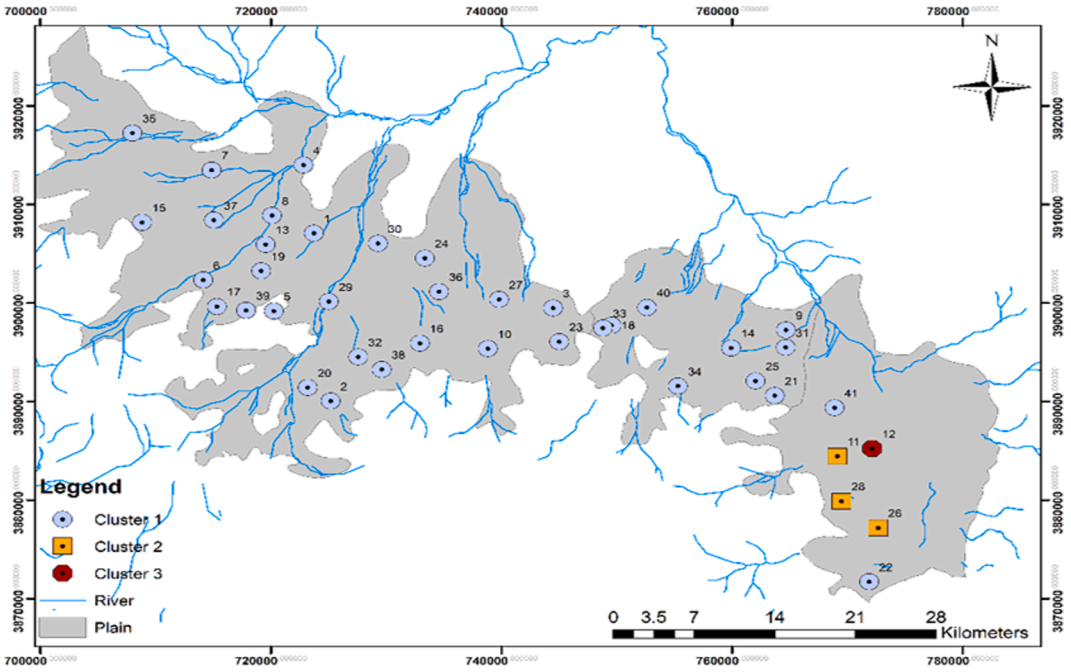

Fig. 13. Spatial distribution of groundwater quality clusters in the fourth-time step.

distinguishable clusters and could visualize the spatiotemporal changes in the PIG.

To classify irrigation water, the USSL suggested a practical diagram that describes the combined effects of sodium hazards and salinity hazards. On the USSL diagram, S and C are the abbreviations for SAR and EC in micromhos per centimeter (Balasubramanian et al., 2015). In this step, the USSL diagram categorizes the clusters for irrigation purposes using SAR and EC values. The USSL plots of groundwater samples illustrate all members in the limits of C2S1 (medium-salinity and low-sodium water) and C3S1 (high-salinity and low-sodium water), suggesting that the groundwater samples were satisfactory for irrigational use in all time steps (Fig. 14).

Comparing the USSL diagrams (Fig. 14) revealed that members of cluster 2 of the second-time step experienced a noticeable increase in associated variables (EC and SAR) in the next time steps. Consequently, some of the members entered the C3S1 status due to their movements in the USSL diagrams. Eventually, cluster 3, with only one member, is bound to fall into the C4S1 (very high salinity with low sodium) zone in the fourth-time step. Overall, the USSL diagrams of all time steps illustrated that most parts of the GDP had a satisfactory quality for irrigation, while the continuous increases in physicochemical variables in the eastern part of the plain decreased the suitability of groundwater for irrigational purposes.

To gain a broader perspective regarding temporal changes in physicochemical variables, the PIG, SAR, EC, GWL, and SC values of centroid wells are plotted in Fig. 15 as representatives of groundwater quality in various regions of the plain. Due to the different units of variables, they were normalized before plotting.

Regarding Fig. 15b, well 24 was selected as the representative of the western cluster for groundwater quality and this monitoring well experienced unusual changes over time. As shown in Fig. 15b, all variables reached their maximum in the second-time step. Despite this increase, it was still in the category of insignificant pollution and excellent water according to the PIG and USSL diagrams. After the second-time step, despite the sharp decrease in GWL, the trend of quality variables gradually decreased. Consequently, water quality conditions improved in the western part of the GDP based on the PIG and USSL diagrams. The trend of the SC in this quality monitoring well indicates that the increase in the quality variables disturbed the homogeneous structure of the members in the second-time step. However, with the beginning of the decreasing trend of the variables, the SC subsequently began to increase after the third-time step.

For well 28, the maximum increase in quality variables occurred between the third- and fourth-time steps, which caused a low pollution, high salinity, and low sodium status for drinking purposes and irrigational use. Fig. 15c also indicates that the decrease in GWL had an influential role in increasing the concentration of quality variables in this area. Investigating the increasing trend of the SC for well 28 during the time steps illustrates that the increase in quality variables in the second and third steps formed more homogeneous clusters that reveal spreading pollution in groundwater in the eastern part of the GDP.

The highest concentration of qualitative variables could be observed in the eastern part of the GDP, and well 12 was the centroid member of the most critical clusters in all time steps, which has undergone sharp increases in physicochemical variables (see Fig. 15a). Due to this escalation during the fourth-time step, this well could not be placed with any of the other clusters and thus formed a single-member cluster. During the last-time step, experiencing an 83% increase in SAR and a 130% increase in EC, this well was bound to fall into the C4S1 zone, indicating very high salinity, which represents an alarming condition for this type of water that is used for irrigation purposes. The PIG of well 12 did not experience considerable fluctuations in the first three time steps, but with an increase of 150%, it was categorized as highly polluted for drinking purposes in the fourth period.

Finally, the eastern part of the plain with a noticeable increase in quality variables was recognized as the area undergoing the most changes in groundwater quality variables, while the highest groundwater depletion rate occurred in the western part of the GDP.

4.6. *Scenarios for the groundwater quality in the eastern part of GDP*

Different scenarios are considered to explore the significant reasons for the detected critical clusters in eastern GDP based on the outcomes of statistical approaches in this study.

In the first scenario, to investigate the effects of the aquifer's essence, geological explorations in the structure of the aquifer were performed. The sediment, cementing materials, different minerals, and lithostratigraphy units have particular properties to erosion and weathering.

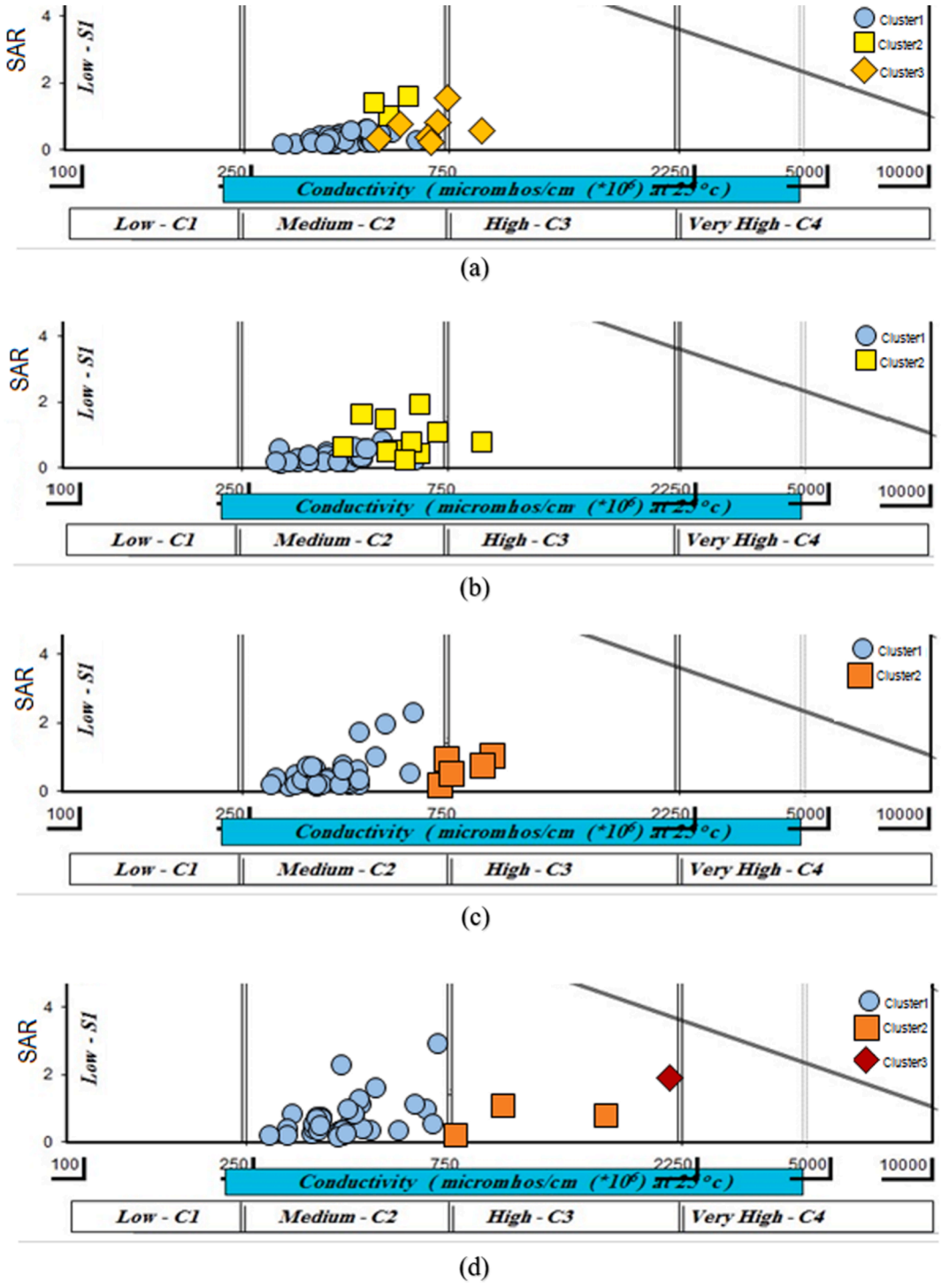

Fig. 14. The USSL diagrams in the (a) first, (b) second, (c) third, and (d) fourth-time steps.

According to the kind of petrology of each formation, water may dissolve different cations and anions, which finally changes the quality of water. Evaporated deposits such as gypsum, anhydrite, marl, and salts are sensitive to erosion and weathering. So, toxic ions such as Cl^{-}, SO_4^{2-} and Na^{+} can separate from them easily and decrease the quality of water. The results of hydrogeological investigations (section 2) indicated that the eastern part of GDP consists of fine-grained alluvial deposits with high percents of silt, clay, and gravel at the first layers (Fig. 3d), and its bedrock is an alternation of marl rocks which may have an influential rule in decreasing the groundwater quality which is consistent with previous studies (e.g., Rahmati et al., 2015). Also, other studies indicated that the ground slope is an influential factor affecting the groundwater quality because, in slow slopes, surface water pollution has enough time to penetrate into the underground (e.g., Nadiri et al., 2017; Chen et al., 2019). Fig. 3a shows the digital elevation model of GDP that indicates the eastern part of GDP has slow slopes compared with other parts of the plain, which may affect groundwater quality by penetrating the agricultural pollution into the ground.

Another scenario is the effects of the groundwater flow path; Alluvial deposits of a plain can be an important source of groundwater. The geology of GDP (Figs. 2 and 3) has a great potential for precipitation and irrigation return flow infiltration. Also, the existence of limestone and

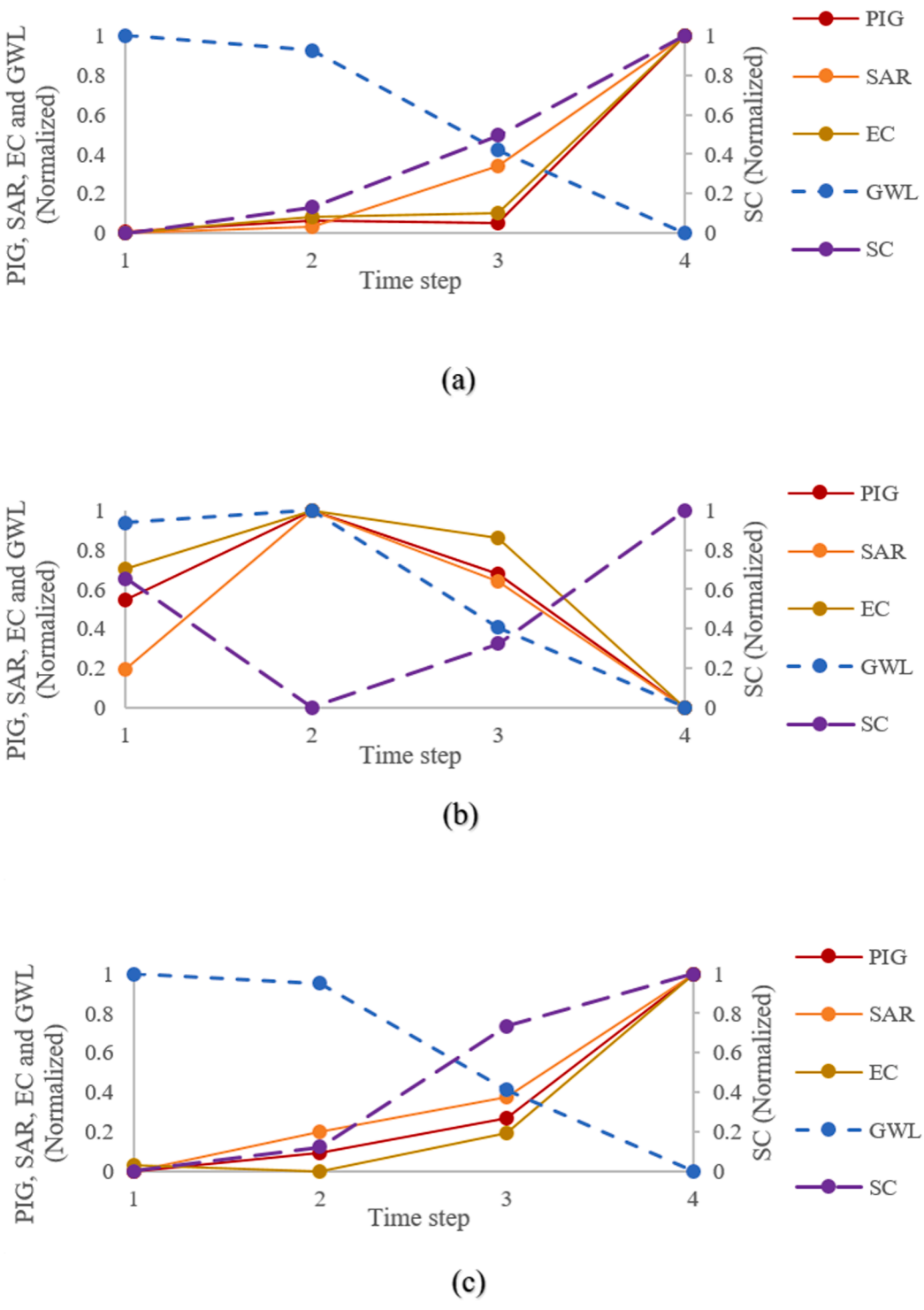

Fig. 15. The temporal changes of the PIG, SAR, EC, GWL and SC of centroid wells in quality clustering: (a) W12, (b) W24, and (c) W28.

dolomite in some parts of the plain show karst systems that are characterized as regions with high pollution vulnerability. The dominant groundwater flow direction of GDP is from the west and southwestern parts of the plain to the east and southeastern regions (Fig. 5). The direction of groundwater flow can explain the spatial distribution of quality clusters. Figs. 5 and 13 illustrate that the polluted clusters of the aquifer have spread in the direction of the groundwater flow path of the eastern part of GDP. Also, a lower hydraulic gradient in the eastern part of the plain can be a reason for high concentrations of groundwater quality variables. According to the Chebotarev sequence (Chebotarev, 1955), as water moves in the direction of the flow path, the chemical composition experiences normal changes. Changes in water quality composition also occur with increasing depth of travel, as bicarbonate anions, which dominate in many shallow groundwaters, give way to

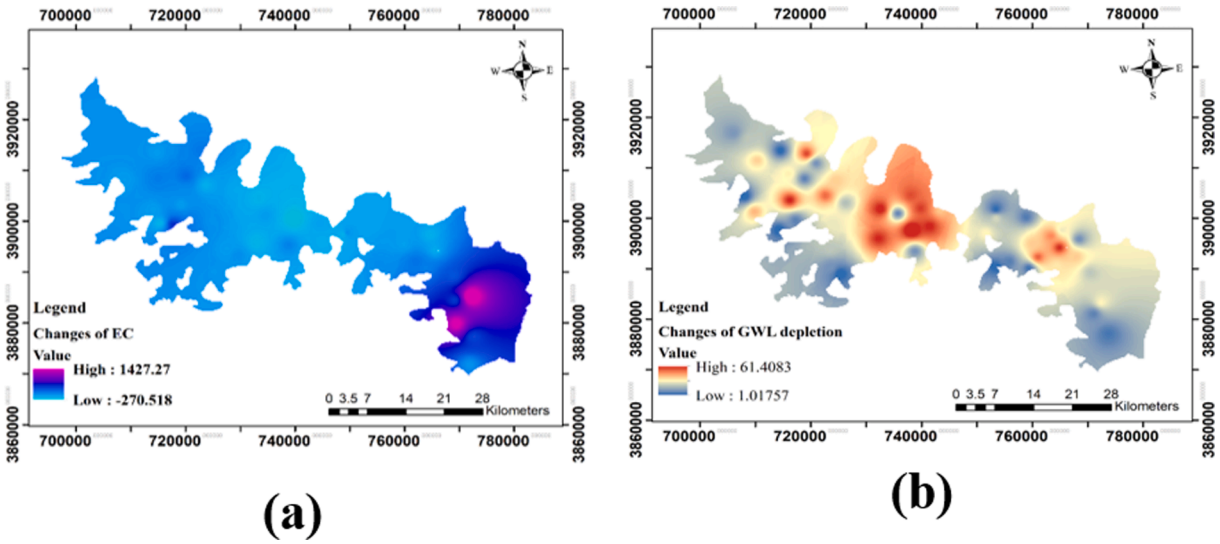

Fig. 16. The distribution of changes in (a) EC and (b) groundwater depletion.

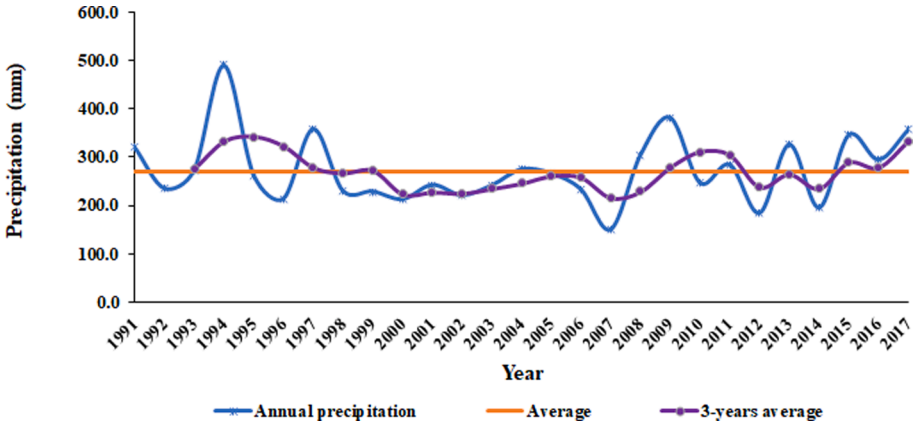

Fig. 17. The wet and dry periods of the eastern part of GDP.

sulfate and then chloride anions, and calcium is exchanged for sodium. In this study, the groundwater flow path may result in more EC values in the eastern parts regarding the Chebotarev sequence.

Anthropogenic activities can be another cause that forced groundwater quality of GDP with significant problems. The results of section 4.3 showed that GDP experienced a sharp increase in the area of irrigated croplands that require large amounts of water, fertilizers, and pesticides to achieve high production. There can be a significant relationship between cropland expansion and groundwater quality of GDP, which was also presented by other studies (e.g., Rahmati et al., 2015).

The effect of changes in the groundwater depletion on values of EC might be considered as another scenario. Therefore, the correlation coefficient between the changes of EC and groundwater depletion was estimated. The results showed a low negative correlation (-0.21), indicating that changes in groundwater depletion and EC values did not contain considerable linkage (see Fig. 16).

In another scenario, the moving average method was utilized to study annual precipitation data in the meteorological station (P5 in Fig. 1a) located in the eastern GDP (see Fig. 17). The results denoted that this part of the plain experienced dry periods from 1999 to 2009, and from 2012 to 2015, which can affect the groundwater quality.

Finally, the eastern part of the plain with a noticeable increase in physicochemical variables such as EC was recognized as the area undergoing the most changes in groundwater quality variables, while the highest groundwater depletion rate occurred in the western part of the GDP. Taken together, aquifer materials, low rate of recharge, slow slope, groundwater flow path, the increasing trends of groundwater depletion, occurring multiple dry periods, cropland area expansion, overuse of chemical fertilizers and pesticides in the eastern part of GDP are the influential factors that affect the groundwater quality.

5. Conclusions

In the present study, long-term spatiotemporal assessment of groundwater quantity and quality on the GDP was conducted using a combination of results from three different types of clustering methods. Furthermore, to fulfill the aim of extracting the most homogeneous clusters, a cluster ensemble method was applied. Ensemble clustering enhanced the final validity index in quantitative and qualitative groundwater clustering up to 12% and 20%, respectively.

The significant increase in irrigated cropland area and the changes of crop patterns relating to the cultivation of water-intensive crops, such as potatoes and forage, in the eastern part of the GDP caused large declines in GWL (almost 26 m) and an increase in groundwater quality variables in clusters that represents a shift from insignificant pollution to low and high pollution in the last-time step. Furthermore, the patterns of GWL revealed that the most noticeable groundwater depletion (almost 33 m) occurred in cluster 7, which is located in the western part of the GDP, which has had a considerable increase in cropland area between the first- and last-time steps. The final results revealed that simultaneous

analysis of the cluster ensemble with the USSL diagram, Piper plot, and PIG is a flexible and scientifically justified approach to recognize and display the changing patterns of groundwater quantity and quality. The results of this study provide insight into the spatiotemporal changes in groundwater conditions on the GDP that can be utilized for long-term policies and effective implementation of mitigation measures.

For future studies, combining the cluster ensemble method with artificial intelligence approaches to forecast groundwater quantity and quality variables is proposed. Due to the lack of monthly physico-chemical data for the study area, groundwater quality clustering was performed using 6-monthly data, and it would be more efficient to apply the proposed methodology to other study areas with monthly physico-chemical datasets, if available. Furthermore, the spatiotemporal cluster ensemble method of hydroclimatological variables is also suggested to recognize the impacts of climate change.

CRediT authorship contribution statement

Vahid Nourani: Conceptualization, Supervision, Methodology, Writing – review & editing. **Parnian Ghaneei:** Project administration, Methodology. **Sameh A. Kantoush:** Validation, Formal analysis, Writing – review & editing.

Declaration of Competing Interest

The authors declare that they have no known competing financial interests or personal relationships that could have appeared to influence the work reported in this paper.

Acknowledgement

This work was funded by APN "Asia-Pacific Network for Global Change Research" under project reference number CRRP2020-09MY-Kantoush (Funder ID: https://doi.org/10.13039/100005536).

References

Abdi, A., Hassanzadeh, Y., Ouarda, T.B., 2017. Regional frequency analysis using Growing Neural Gas network. J. Hydrol. 550, 92–102.

Aljobouri, H.K., Jabera, H.A., Kocak, O.M., Algin, O., Cnkayaa, I., 2018. Clustering fMRI data with a robust unsupervised learning algorithm for neuroscience data mining. J. Neurosci. Methods 299, 45–54.

Alqurashi, T., Wang, W., 2019. Clustering ensemble method. Int. J. Mach. Learn. Cybern. 10, 1227–1246.

Azimi, J., Cull, P., Fern, X., 2009. Clustering Ensembles Using Ants Algorithm, Methods and Models in Artificial and Natural Computation. A Homage to Professor Mira's Scientific Legacy. pp: 295–304.

Baghanam, A.H., Nourani, V., Aslani, H., Taghipour, H., 2020. Spatiotemporal variation of water pollution near landfill site: application of clustering methods to assess the admissibility of LWPI. J. Hydrol. 591, 125581. https://doi.org/10.1016/j.jhydrol.2020.125581.

Balasubramanian, N., Sivasubramanian, P., Soundranayagam, J.P., Chandrasekar, N., Gowtham, B., 2015. Groundwater classification and its suitability in Kadaladi, Ramanathapuram, India using GIS techniques. Environ. Earth Sci. 74, 3263–3285.

Bhakar, P., Singh, A.P., 2019. Groundwater quality assessment in a hyper-arid region of Rajasthan, India. Nat. Resour. Res. 28.

Chebotarev, I.I., 1955. Metamorphism of natural waters in the crust of weathering—1. Geochim. Cosmochim. Acta Vol. 8.

Chen, W., Panahi, M., Khosravi, K., Reza, H., Rezaie, F., 2019. Spatial prediction of groundwater potentiality using ANFIS ensembled with teaching-learning-based and biogeography-based optimization. J. Hydrol. 572.

Egbueri, J.C., 2020. Groundwater quality assessment using pollution index of groundwater (PIG), ecological risk index (ERI) and hierarchical cluster analysis (HCA): a case study. Groundwater Sustainable Dev. 10, 100292.

Fabbrocino, S., Rainieri, C., Paduano, P., Ricciardi, A., 2019. Cluster analysis for groundwater classification in multi-aquifer systems based on a novel correlation index. J. Geochem. Explor. 204, 90–111.

Foroumandi, E., Nourani, V., Sharghi, E., 2021. Climate change or regional human impacts? remote sensing tools, artificial neural networks, and wavelet approaches aim to solve the problem. Hydrol. Res. 52 (1), 176–195.

Foroumandi, E., Nourani, V., Kantoush, S.A., 2022. Investigating the main reasons for the tragedy of large saline lakes: drought, climate change, or anthropogenic activities? a call to action. J. Arid Environ. 196, 104652. https://doi.org/10.1016/j.jaridenv.2021.104652.

Fritzke, B., 1995. A growing neural gas network learns topologies. MIT Press 7, 625–632.

García-RodríGuez, J., Angelopoulou, A., García-Chamizo, J.M., Psarrou, A., Escolano, S. O., Giménez, V.M., 2012. Autonomous Growing Neural Gas for applications with time constraint: optimal parameter estimation. Neural Networks. 32, 196–208.

Jimeno-Morenilla, A., Garcia-Rodriguez, J., Orts-Escolano, S., Davia-Aracil, M., 2013. 3D-based reconstruction using growing neural gas landmark: application to rapid prototyping in shoe last manufacturing. Int. J. Adv. Manuf. Technol. 69, 657–668.

Kurdistan Regional Water Authority, KRWA, (2017). Extended the prohibition of Ghorveh Dehgolan plain aquifer, Final report.

MacQueen, J.B., 1967. Some methods for classification and analysis of multivariate observations. Proceedings of 5th Berkeley Symposium on Mathematical Statistics and Probability. *University of California Press.* pp: 281–297.

Mimaroglu, S., Erdil, E., 2011. Combining multiple clustering using similarity graph. Pattern Recogn. 44, 694–703.

Mimaroglu, S., Erdil, E., 2013. An efficient and scalable family of algorithms for combining clustering. Eng. Appl. Artif. Intell. 26, 2525–2539.

Mohammadi, M., Nikanjam, A., Rahmani, A., 2008. An evolutionary approach to clustering ensemble. In: Proceedings of the 2008 Fourth International Conference on Natural Computation. IEEE Computer Society, Washington, DC, USA, pp. 77–82.

Nadiri, A.A., Gharekhani, M., Khatibi, R., Sadeghfam, S., Moghaddam, A.A., 2017. Groundwater vulnerability indices conditioned by Supervised Intelligence Committee Machine (SICM). Sci. Total Environ. 574, 691–706.

Nourani, V., Kalantari, O., 2010. Integrated artificial neural network for spatiotemporal modeling of rainfall-runoff-sediment process. Environ. Eng. Sci. 27 (5), 411–422.

Nourani, V., Alami, M.T., Daneshvar, F., 2016. Self-organizing map clustering technique for ANN-based spatiotemporal modeling of groundwater quality parameters. J. Hydroinf. 18 (2), 288–309.

Nourani, V., Foroumandi, E., Sharghi, E., Dąbrowska, D., 2021. Ecological-environmental quality estimation using remote sensing and combined artificial intelligence techniques. J. Hydroinf. 23 (1), 47–65.

Piper, A.M., 1994. A graphical procedure in the geochemical interpretation of water analysis. Trans. Am. Geophys. Union 25, 914–928.

Rahmati, O., Samani, A.N., Mahmoodi, N., Mahdavi, M., 2015. Assessment of the contribution of N-fertilizers to nitrate pollution of groundwater in western Iran (case study Ghorveh-Dehgelan Aquifer). Water Quality Exposure Health 7.

Rousseeuw, P.J., 1987. Silhouettes: a graphical aid to the interpretation and validation of cluster analysis. J. Comput. Appl. Math. 20, 53–65.

Santos, C.P., Nascimento, M.C.V., 2016. Growing Neural Gas as a memory mechanism of a heuristic to solve a community detection problem in networks. Procedia Comput. Sci. 96.

Sharif, S.M., Kusin, F.M., Asha'ari, Z.H., Aris, A.Z., 2015. Characterization of water quality conditions in the klang river basin, malaysia using self organizing map and K-means algorithm. Procedia Environ. Sci. 30.

Shi, J., Chen, C., Zhong, S., 2014. Privacy preserving growing neural gas over arbitrarily partitioned data. Neurocomputing. 144, 427–435.

Subba Rao, N., 2012. PIG: a numerical index for dissemination of groundwater contamination zones. Hydrol. Process. 26, 3344–3350.

Subba Rao, N., Chaudhary, M., 2019. Hydrogeochemical processes regulating the spatial distribution of groundwater contamination, using pollution index of groundwater (PIG) and hierarchical cluster analysis (HCA): a case study. Groundwater Sustainable Dev. 9, 100238.

Viejo, D., Garcia-Rodriguez, J., Cazorla, M., 2014. Combining visual features and Growing Neural Gas networks for robotic 3D SLAM. Inf. Sci. 276, 174–185.

Wu, C., Fang, C., Wu, X., Zhu, G., Zhang, Y., 2021. Hydrogeochemical characterization and quality assessment of groundwater using self-organizing maps in the Hangjinqi gasfield area, Ordos Basin, NW China. Geosci. Front. 12 (2), 781–790.